Strong-coupling expansion for the momentum distribution of the Bose-Hubbard model with benchmarking against exact numerical results

J. K. Freericks,[1] H. R. Krishnamurthy,[1,2,3] Yasuyuki Kato,[4] Naoki Kawashima,[4] and Nandini Trivedi[5]

[1]*Department of Physics, Georgetown University, 37th and O Streets NW, Washington, D.C. 20057, USA*

[2]*Centre for Condensed Matter Theory, Department of Physics, Indian Institute of Science, Bangalore 560012, India*

[3]*Condensed Matter Theory Unit, Jawaharlal Nehru Centre for Advanced Scientific Research, Bangalore 560064, India*

[4]*Institute for Solid State Physics, University of Tokyo, Kashiwa, Chiba 277-8581, Japan*

[5]*Department of Physics, The Ohio State University, Columbus, Ohio 43210, USA*

A strong-coupling expansion for the Green's functions, self-energies, and correlation functions of the Bose-Hubbard model is developed. We illustrate the general formalism, which includes all possible (normal-phase) inhomogeneous effects in the formalism, such as disorder or a trap potential, as well as effects of thermal excitations. The expansion is then employed to calculate the momentum distribution of the bosons in the Mott phase for an infinite homogeneous periodic system at zero temperature through third order in the hopping. By using scaling theory for the critical behavior at zero momentum and at the critical value of the hopping for the Mott insulator–to–superfluid transition along with a generalization of the random-phase-approximation-like form for the momentum distribution, we are able to extrapolate the series to infinite order and produce very accurate quantitative results for the momentum distribution in a simple functional form for one, two, and three dimensions. The accuracy is better in higher dimensions and is on the order of a few percent relative error everywhere except close to the critical value of the hopping divided by the on-site repulsion. In addition, we find simple phenomenological expressions for the Mott-phase lobes in two and three dimensions which are much more accurate than the truncated strong-coupling expansions and any other analytic approximation we are aware of. The strong-coupling expansions and scaling-theory results are benchmarked against numerically exact quantum Monte Carlo simulations in two and three dimensions and against density-matrix renormalization-group calculations in one dimension. These analytic expressions will be useful for quick comparison of experimental results to theory and in many cases can bypass the need for expensive numerical simulations.

I. INTRODUCTION

The Bose-Hubbard model [1–3] was heavily studied as a simple model for disordered superconductors [2]. Subsequently it was demonstrated [4] that ultracold atoms trapped in optical lattices provide an alternate, and more controllable, experimental realization of it, sparking even more interest. One of the most useful tools for analyzing the states of cold-atom systems is a time-of-flight measurement of their momentum distribution when the lattice and trapping potentials are rapidly shut off and the atomic cloud is allowed to expand and then is imaged with absorption spectroscopy [5]. The time-of-flight image, in the long-expansion-time limit, is directly related to the momentum distribution function of the atoms in the optical lattice before expansion [6,7].

Even before cold-atom systems were employed to examine Bose-Hubbard model physics, the phase diagram of the model was accurately determined in a strong-coupling approximation [8,9] (for a recent review of this early history, see Ref. [10]). This approach, which relied on expanding the properties in a perturbative series in the hopping, captured much of the behavior of the model, and when extrapolated via a scaling-theory ansatz for the critical behavior at the tips of the Mott lobes [2], proved to be as accurate as the quantum Monte Carlo (QMC) simulations that had been performed at that time [11,12]. Since then, the strong-coupling perturbation theory has been pushed to higher order [13–15],

and the QMC simulations have improved dramatically in two [16] and three dimensions [17,18]. In addition, highly accurate density-matrix renormalization-group (DMRG) studies have been performed on the model in one dimension [19–21].

Surprisingly, despite all of the work that has been performed on the phase diagrams with a strong-coupling analysis, there are only limited results for the momentum distribution functions. The first few terms of the structure factor have been determined to high order in one dimension [15] and the zero-momentum distribution function has been examined in one and two dimensions [14]. A recent random-phase approximation (RPA) has been carried out [22], which corresponds to the exact solution for the momentum distribution in the infinite-dimensional limit (see also Ref. [23]). In this contribution, we present an alternative formulation of the strong-coupling perturbation theory for the many-body Green's functions, which can be immediately employed to evaluate the momentum distribution function as a power series in the hopping divided by the interaction strength for each value of the momentum. Recently a similar strong-coupling formalism to ours has been proposed [24] and used to calculate the momentum distribution in three dimensions through second order [25]. We take our strong-coupling expansion and, guided by the exact solution from the RPA, we *construct an ansatz* for the scaling behavior of the momentum distribution function and then employ it to produce *ana-*

lytic expressions for the momentum distribution that we believe *are accurate for all values* of the hopping within the Mott phase in two and three dimensions. These results could prove useful as a simple means to check against experimental data on more recent Bose-Hubbard model systems [26–28]. We also take the results for the scaling behavior of the momentum distribution and use it as a phenomenological ansatz for the scaling behavior of the phase diagram that sums many more terms than the original ansatz. Comparing that result with the QMC data in two and three dimensions also shows excellent agreement. It is not clear at this stage whether the QMC data for the phase boundary or the scaled (phenomenological) form of the strong-coupling expansion are more accurate. We also present QMC simulations of the momentum distribution. These QMC simulations represent state-of-the-art calculations on system sizes of up to 64 $\times 64 \times 64$ and up to 1×10^6 particles. They have been obtained using the directed-loop algorithm with continuous imaginary time and with several improvements in the algorithm that have allowed us to explore the large phase space and minimize critical slowing down (these improvements include eliminating one-site and two-body vertices). The accuracy is tested via comparing critical exponents with exact known values.

We write the bosonic Hubbard Hamiltonian in the presence of a potential in the form

$$\mathcal{H} = \mathcal{H}_0 + \mathcal{H}_{hop} = \sum_j \mathcal{H}_{0j} + \mathcal{H}_{hop},$$

$$\mathcal{H}_{0j} \equiv [V_T(\mathbf{r}_j) - \mu]\hat{n}_j + \frac{U}{2}\hat{n}_j(\hat{n}_j - 1), \qquad (1)$$

$$\mathcal{H}_{hop} \equiv -\sum_{j,j'} \mathsf{t}_{jj'} a_j^\dagger a_{j'}. \qquad (2)$$

Here j, j' label the sites of a (hypercubic) lattice in d dimensions, with a lattice constant which we set equal to 1 (the unit of distance); $\mathbf{r}_j$ is the position vector of the jth site as measured from the center of the system. The symbols $a_j^\dagger$ and a_j denote creation and destruction operators for bosons at lattice site j. These operators obey the commutation relation $[a_{j'}, a_j^\dagger] = \delta_{j'j}$; $\hat{n}_j = a_j^\dagger a_j$ is the boson number operator at site j. $V_T(\mathbf{r}_j)$ is the trap potential (which is usually assumed to be a simple harmonic-oscillator potential) and the repulsive contact interaction is given by U. Note that the trapping potential could also represent a diagonal disorder potential, if desired, but we will not discuss that case further here. The chemical potential μ controls the average number of particles. $\mathsf{t}_{jj'}$ is the amplitude for bosons to hop from site j' to site j. We consider a general $\mathsf{t}_{jj'}$ for the formal developments we present in the earlier parts of the paper, but later specialize to the case of nearest-neighbor hopping only, with amplitude t, on a hypercubic lattice in d dimensions. Because it takes only a little more work to provide results for the general case of a trap (or diagonal disorder) potential, we proceed with the formal developments in full generality. But our application of these formulas here will be only for the

homogeneous-lattice case with no trap potential and no disorder.

As explained above, our aim in this paper is to calculate the properties of the Hamiltonian in Eq. (2), in particular, its momentum distribution function. The momentum distribution function is related to the atom-atom correlation function [see Eq. (6)] involving atoms at sites j and j', which is given by

$$C_{j'j} = \langle a_{j'}^\dagger a_j \rangle_{\mathcal{H}}, \quad \langle \mathcal{A} \rangle_{\mathcal{H}} \equiv Z^{-1} \operatorname{Tr}[\mathcal{A}e^{-\beta\mathcal{H}}]. \qquad (3)$$

This expectation value can be calculated from the single-particle "thermal" or "Matsubara" Green's function, defined in the standard way [29], as

$$G_{jj'}(\tau, \tau') \equiv -\langle \mathcal{T}_\tau[e^{\tau\mathcal{H}}a_j e^{-\tau\mathcal{H}} e^{\tau'\mathcal{H}} a_{j'}^\dagger e^{-\tau'\mathcal{H}}] \rangle_{\mathcal{H}}, \qquad (4)$$

by choosing $\tau = 0$ and $\tau' = 0^+$, the positive infinitesimal; i.e.,

$$C_{j'j} = -G_{jj'}(0, 0^+). \qquad (5)$$

Here, as usual, $\beta \equiv 1/k_B T$ is the inverse temperature, $0 < \tau < \beta$ and $0 < \tau' < \beta$ are "imaginary time" variables, $\mathcal{T}_\tau$ is the imaginary time-ordering operator, and $Z \equiv \operatorname{Tr}[e^{-\beta\mathcal{H}}]$ is the partition function. The momentum distribution function measured in the time-of-flight experiments is proportional to the Fourier transform of the atom-atom correlation function:

$$n_\mathbf{k} \equiv \frac{1}{\mathcal{N}} \sum_{j,j'} C_{j'j} e^{i\mathbf{k} \cdot (\mathbf{r}_{j'} - \mathbf{r}_j)}, \qquad (6)$$

where $\mathcal{N}$ is the number of sites in the lattice. (We do not discuss the proportionality factors, which arise from the Wannier wave functions of the trapped atoms, as these are not germane to the work we present here.)

Specializing to the case of nearest-neighbor hopping on a hypercubic lattice in d dimensions, we report our main result which is the general strong-coupling expansion for the ($T = 0$) momentum distribution of the Mott phase with a density n up to third order in the hopping:

$$
\begin{aligned}
n_\mathbf{k} = n\Bigg\{ &1 - 2(n+1)\frac{\epsilon_\mathbf{k}}{U} + 3(n+1)(2n+1) \\
&\times \left[\left(\frac{\epsilon_\mathbf{k}}{U}\right)^2 - 2d\left(\frac{\mathsf{t}}{U}\right)^2\right] - 4(n+1)[5n^2 + 5n + 1]\left(\frac{\epsilon_\mathbf{k}}{U}\right)^3 \\
&+ \left[\frac{2}{3}(n+1)(26n^2 + 26n + 5)\right]4d\left(\frac{\epsilon_\mathbf{k}\mathsf{t}^2}{U^3}\right) \\
&- \left[\frac{1}{3}(n+1)(23n^2 + 23n + 2)\right]\left(\frac{\epsilon_\mathbf{k}\mathsf{t}^2}{U^3}\right)\Bigg\}, \qquad (7)
\end{aligned}
$$

where $\epsilon_\mathbf{k} = -\mathsf{t}\sum_\delta \exp[i\mathbf{k} \cdot \delta]$ is the band structure, δ is a nearest-neighbor translation vector, and d is the spatial dimension. Note that we do not present any results within the superfluid phase. It is possible to generalize the Green's-function formalism to include the anomalous diagrams present in the superfluid state, but we have not yet completed that analysis.

Readers who are mainly interested in seeing how accurate this expansion is when applied to explicit cases are encouraged to skip Sec. II, which develops the formal techniques

needed for obtaining the expansion, and proceed directly to Sec. III, where we use the expansion to develop a scaling analysis and compare results to exact numerics.

The paper is organized as follows. In Sec. II, we present the formalism for the strong-coupling expansion of the Green's functions and produce explicit formulas through third order for the one-dimensional lattice, the two-dimensional square lattice, and the three-dimensional cubic lattice, along with the infinite-dimensional hypercubic lattice. In Sec. III, we present our scaling analysis for the momentum distribution in the first Mott lobe and compare those results to available numerical data from QMC and DMRG calculations. We also discuss the phenomenological approach to the phase diagram in two and three dimensions. Conclusions and a discussion of future directions follow in Sec. IV. Appendixes A and B contain some of the more technical results.

II. STRONG-COUPLING FORMALISM FOR THE GREEN'S FUNCTIONS

The strong-coupling expansion we develop in this paper enables one to calculate $G_{jj'}$ [in Eq. (4)], and hence $C_{j'j}$ [in Eq. (5)], as an expansion in powers of $\mathcal{H}_{hop}$ [in Eq. (2)], with respect to regions of the system which are either *normal* or *Mott insulating* (i.e., *not* superfluid). In order to generate expansions about regions with superfluidity, one needs to include a breakup of the hopping term that allows for non-zero values of the expectation values $\langle a_j^\dagger \rangle$ and $\langle a_j \rangle$, as in the mean-field treatment of the Bose-Hubbard model [3], into the relevant piece of $\mathcal{H}_{0j}$. The resulting terms are more complicated than the ones discussed here, involving anomalous multiparticle single-site Green's functions (including those with an odd number of creation/destruction operators). We hope to discuss these types of terms in future work. For now, we focus on the normal and Mott-insulating phases and we use the following standard relation [29] to define the imaginary time-ordered product for the evolution operator in the "interaction picture:"

$$e^{-\tau\mathcal{H}}e^{\tau'\mathcal{H}} = e^{-\tau\mathcal{H}_0}\mathcal{U}(\tau,\tau')e^{\tau'\mathcal{H}_0}, \qquad (8)$$

$$\mathcal{U}(\tau,\tau') \equiv \mathcal{T}_\tau \exp\left[-\int_{\tau'}^{\tau} d\tau_1 \mathcal{H}_{hop}(\tau_1)\right], \qquad (9)$$

where for any operator $\mathcal{A}$, we define the time-dependent operator $\mathcal{A}(\tau_1) \equiv e^{\tau_1\mathcal{H}_0}\mathcal{A}e^{-\tau_1\mathcal{H}_0}$. Using the properties of $\mathcal{T}_\tau$, and the rules for composition for products of $\mathcal{U}$, it is straightforward to show that [29]

$$G_{jj'}(\tau,\tau') = -\frac{\langle\mathcal{T}_\tau[\mathcal{U}(\beta,0)a_j(\tau)a_{j'}^\dagger(\tau')]\rangle_{\mathcal{H}_0}}{\langle\mathcal{U}(\beta,0)\rangle_{\mathcal{H}_0}}. \qquad (10)$$

The strong-coupling expansion we use in this paper is obtained straightforwardly by expanding the exponentials in $\mathcal{U}$ [in Eq. (10)] in powers of $\mathcal{H}_{hop}$ and evaluating the resulting traces with respect to the equilibrium ensemble of $\mathcal{H}_0$. The term of order m in such an expansion for the *numerator* in Eq. (10) is given by

$$\frac{1}{m!}\sum_{j_m j_m'}\cdots\sum_{j_1 j_1'}\int_0^\beta d\tau_m\cdots\int_0^\beta d\tau_1 \mathsf{t}_{j_m j_m'}\cdots\mathsf{t}_{j_1 j_1'}$$

$$\times \langle\mathcal{T}_\tau[a_j(\tau)a_{j_m}^\dagger(\tau_m^+)a_{j_m'}(\tau_m)\cdots a_{j_1}^\dagger(\tau_1^+)a_{j_1'}(\tau_1)a_{j'}^\dagger(\tau')]\rangle_{\mathcal{H}_0}. \qquad (11)$$

Since $\mathcal{H}_0$, as defined in Eq. (2), is a sum of separate terms for each site, the thermal average in Eq. (11) factorizes into a product of factors, one for each of the sites on the lattice, in terms of the multiparticle single-site Green's functions at these sites defined in the standard way [29] as

$$\mathcal{G}_j(\tau_1,\tau_1') \equiv -\langle\mathcal{T}_\tau[a_j(\tau_1)a_j^\dagger(\tau_1')]\rangle_{\mathcal{H}_{0j}}, \qquad (12)$$

$$\mathcal{G}_j^{II}(\tau_1,\tau_2;\tau_2',\tau_1') \equiv \langle\mathcal{T}_\tau[a_j(\tau_1)a_j(\tau_2)a_j^\dagger(\tau_2')a_j^\dagger(\tau_1')]\rangle_{\mathcal{H}_{0j}},$$

$$\vdots \qquad (13)$$

Note that these are total Green's functions, containing both connected and disconnected parts. Furthermore, each site that appears must occur an even number of times in the thermal average, half as indices of creation operators and half as indices of destruction operators. (This restriction would change if one included the possibility of superfluidity, which we reserve for future work.) Similar considerations apply to the terms in the expansion for the denominator in Eq. (10) [except for the absence of the operators $a_j(\tau)$ and $a_{j'}^\dagger(\tau')$]. As we discuss in more detail below, the combination of the two expansions order by order leads to a cancelation of all "disconnected" terms, i.e., those involving products of thermal averages for clusters of sites that are not connected via hopping matrix elements to the sites j and j', as well as to the fact that the remaining terms can be written entirely in terms of the "connected" or "cumulant" multiparticle Green's functions, corresponding to the well-known linked-cluster theorem [29].

Using the above considerations, it is straightforward to write down systematically the terms in the strong-coupling expansion for $G_{jj'}(\tau,\tau')$. We denote the mth-order contributions with a superscript (m). The different terms contributing in mth order can also be associated with "diagrams," which correspond to lattice "walks" or "world lines" for a particle which starts from site j' at imaginary time τ' and reaches site j at imaginary time τ after m steps (with each "step" corresponding to a hop along the lattice; e.g., from site j_1' to site j_1 induced by $\mathsf{t}_{j_1 j_1'}$, and in between the steps, the particle undergoes imaginary time "evolution," which proceeds either forward or backward in imaginary time). These processes are shown graphically in Figs. 1 and 2. These diagrams are the strong-coupling analogs of the standard diagrams of many-body perturbation theory [29], from which, after some practice, the terms can be written down by inspection. A p-particle Green's function at a particular site appears when a walk visits that site p times. For $m \geq 2$, as we show below, the contributions can be classified further according to a hierarchy of decreasing powers of $1/z$, where z is the coordination number of the lattice, by recombining contributions from intersecting and nonintersecting walks, and we denote
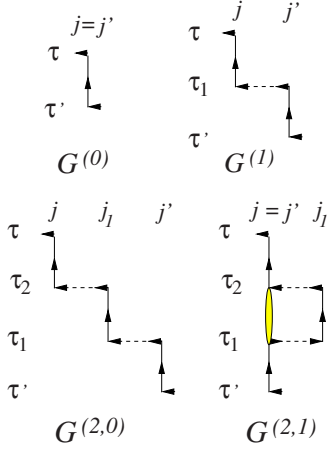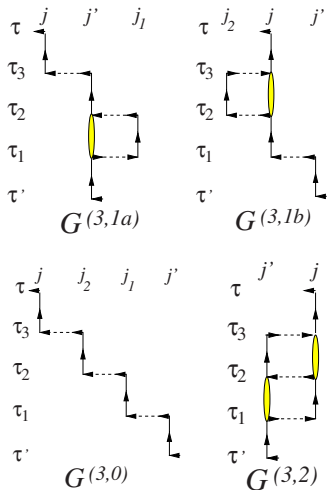
FIG. 1. (Color online) Strong-coupling diagrams for the single-particle Green's functions up to second order in t. The horizontal directed dashed lines indicate the hopping matrix element t between the sites labeled, and the vertical lines indicate single-site Green's functions $\mathcal{G}$ evolving between the respective imaginary times. The ellipse (yellow online) at multiply visited sites denotes the appearance of connected or cumulant n-particle Green's functions.

these with further superscripts as $(m;0),(m;1),\ldots$. We give below the terms contributing to $G_{jj'}(\tau,\tau')$ up to third order in $\mathcal{H}_{hop}$, and their associated strong-coupling diagrams.

The zeroth- and first-order terms are almost obvious,

$$G_{jj'}^{(0)}(\tau,\tau') = \delta_{jj'}\mathcal{G}_j(\tau,\tau'), \tag{14}$$

FIG. 2. (Color online) Strong-coupling diagrams for the single-particle Green's functions corresponding to third order in t. The horizontal directed dashed lines indicate the hopping matrix element t between the sites labeled, and the vertical lines indicate single-site Green's functions $\mathcal{G}$ evolving between the respective imaginary times. The ellipses (yellow online) at multiply visited sites denote the appearance of connected or cumulant n-particle Green's functions.

$$G_{jj'}^{(1)}(\tau,\tau') = -\mathsf{t}_{jj'}\int_{\tau_1}\mathcal{G}_j(\tau,\tau_1)\mathcal{G}_{j'}(\tau_1,\tau') \equiv -\mathfrak{G}_{jj'}^{(1)}(\tau,\tau'). \tag{15}$$

Here, and below, for notational convenience we denote integrals over imaginary times by integral symbols with subscripts, rather than by the standard notation. To second order, a two-step lattice walk can either move to a distinct site two steps away or return to the starting site. Hence we get two terms from the numerator of Eq. (10); Eqs. (16) and (17) are when the hop is to a different lattice site, and Eqs. (18) and (19) are when the hop returns back to the original lattice site:

$$G_{jj'}^{(2;a)}(\tau,\tau')_{num} = (1-\delta_{jj'})\sum_{j_1}\mathsf{t}_{jj_1}\mathsf{t}_{j_1j'}$$

$$\times \int_{\tau_2}\int_{\tau_1}\mathcal{G}_j(\tau,\tau_2)\mathcal{G}_{j_1}(\tau_2,\tau_1)\mathcal{G}_{j'}(\tau_1,\tau') \tag{16}$$

$$\equiv (1-\delta_{jj'})\sum_{j_1}\mathfrak{G}_{jj_1j'}^{(2)}(\tau,\tau'), \tag{17}$$

$$G_{jj'}^{(2;b)}(\tau,\tau')_{num} = \delta_{jj'}\sum_{j_1}\mathsf{t}_{jj_1}\mathsf{t}_{j_1j}\int_{\tau_2}\int_{\tau_1}\mathcal{G}_j^{II}(\tau,\tau_1;\tau_2,\tau')\mathcal{G}_{j_1}(\tau_2,\tau_1) \tag{18}$$

$$\equiv \delta_{jj'}\sum_{j_1}\overline{\mathfrak{G}}_{jj_1j}^{(2)}(\tau,\tau'), \tag{19}$$

where the subscript *num* denotes that these are the terms coming from the numerator in the expansion for the Green's function.

We have introduced a new notation above, letting $\mathfrak{G}_{j\cdots j'}^{(m)}$ denote the product of *single-particle Green's functions* at the sites that appear in the m-step lattice walk specified by its lattice indices, starting from right to left, together with the corresponding hopping amplitudes, the imaginary time arguments indicating the starting and ending imaginary times, with the m intermediate imaginary times being integrated over. $\overline{\mathfrak{G}}_{j\cdots j'}^{(m)}$ is defined similarly, except that it necessarily involves self-intersecting lattice walks where one or more sites are visited multiple times, and the product involves r-particle Green's functions at a site that is visited r times, with the intermediate imaginary time arguments being determined by the sequence specified in the lattice walk. For any given m-step lattice walk, both $\mathfrak{G}^{(m)}$ and $\overline{\mathfrak{G}}^{(m)}$ can clearly be written down by inspection.

To correctly obtain $G_{jj'}^{(2)}$, we need to subtract from the above two terms the term that arises as the product of the second-order contribution from the denominator of Eq. (10), corresponding to closed-loop lattice walks involving the sites j and j_1, given by

$$\mathcal{Z}_{jj_1}^{(2)} \equiv t_{jj_1} t_{j_1 j} \int_{\tau_2} \int_{\tau_1} \mathcal{G}_j(\tau_1, \tau_2) \mathcal{G}_{j_1}(\tau_2, \tau_1), \qquad (20)$$

and the zeroth-order term from the numerator, namely, $G_{jj'}^{(0)}(\tau, \tau')$. The net result for $G^{(2)}$ can be re-expressed as the sum of the following two contributions:

$$G_{jj'}^{(2;0)}(\tau, \tau') = \sum_{j_1} \mathfrak{G}_{jj_1 j'}^{(2)}(\tau, \tau') \qquad (21)$$

$$G_{jj'}^{(2;1)}(\tau, \tau') = \delta_{jj'} \sum_{j_1} t_{jj_1} t_{j_1 j} \int_{\tau_2} \int_{\tau_1} \widetilde{\mathcal{G}}_j^{II}(\tau, \tau_1; \tau_2, \tau') \mathcal{G}_{j_1}(\tau_2, \tau_1)$$

$$\equiv \delta_{jj'} \sum_{j_1} \widetilde{\mathfrak{G}}_{jj_1 j}^{(2)}(\tau, \tau') \qquad (22)$$

$$= \delta_{jj'} \sum_{j_1} \{ \overline{\mathfrak{G}}_{jj_1 j}^{(2)}(\tau, \tau') - \mathfrak{G}_{jj_1 j}^{(2)}(\tau, \tau')$$

$$- \mathcal{G}_j(\tau, \tau') \mathcal{Z}_{jj_1}^{(2)} \}. \qquad (23)$$

Here

$$\widetilde{\mathcal{G}}_j^{II}(\tau, \tau_1; \tau_2, \tau') \equiv [\mathcal{G}_j^{II}(\tau, \tau_1; \tau_2, \tau') - \mathcal{G}_j(\tau, \tau_2) \mathcal{G}_j(\tau_1, \tau')$$

$$- \mathcal{G}_j(\tau, \tau') \mathcal{G}_j(\tau_1, \tau_2)] \qquad (24)$$

is the *cumulant* or connected part of the two-particle Green's function at site j. $\widetilde{\mathfrak{G}}^{(m)}$ is defined similarly as $\overline{\mathfrak{G}}^{(m)}$ *except that* the multiparticle Green's functions that appear in $\widetilde{\mathfrak{G}}^{(m)}$ are *all* connected Green's functions. Note that the prefactor $\frac{1}{2!}$ present in Eq. (11) no longer appears in the above equations, as it has been canceled by the 2! ways of choosing the two distinct hopping matrix elements in the expansion.

Similarly, the third-order contributions involve three-step walks. From the numerator of Eq. (10) we get the following terms according to the types of walks involved:

$$G_{jj'}^{(3;a)}(\tau, \tau')_{num} = -(1 - \delta_{jj'}) \sum_{j_2, j_1} (1 - \delta_{j_2 j'})(1 - \delta_{jj_1}) t_{jj_2} t_{j_2 j_1} t_{j_1 j'}$$

$$\times \int_{\tau_3} \int_{\tau_2} \int_{\tau_1} \mathcal{G}_j(\tau, \tau_3) \mathcal{G}_{j_2}(\tau_3, \tau_2) \mathcal{G}_{j_1}(\tau_2, \tau_1)$$

$$\times \mathcal{G}_{j'}(\tau_1, \tau'), \qquad (25)$$

$$G_{jj'}^{(3;b)}(\tau, \tau')_{num} = -(1 - \delta_{jj'}) \sum_{j_1} (1 - \delta_{jj_1}) t_{jj_1} t_{j'j_1} t_{j_1 j'}$$

$$\times \int_{\tau_3} \int_{\tau_2} \int_{\tau_1} \mathcal{G}_j(\tau, \tau_3) \mathcal{G}_{j_1}(\tau_2, \tau_1)$$

$$\times \mathcal{G}_{j'}^{II}(\tau_1, \tau_3; \tau_2, \tau')$$

$$- (1 - \delta_{jj'}) \sum_{j_2} (1 - \delta_{j_2 j'}) t_{jj_2} t_{j_2 j} t_{jj'}$$

$$\times \int_{\tau_3} \int_{\tau_2} \int_{\tau_1} \mathcal{G}_j^{II}(\tau, \tau_2; \tau_3, \tau_1) \mathcal{G}_{j_2}(\tau_3, \tau_2)$$

$$\times \mathcal{G}_{j'}(\tau_1, \tau'), \qquad (26)$$

$$G_{jj'}^{(3;c)}(\tau, \tau')_{num} = -\frac{1}{2!}(1 - \delta_{jj'}) t_{jj'} t_{j'j} t_{jj'}$$

$$\times \int_{\tau_3} \int_{\tau_2} \int_{\tau_1} \mathcal{G}_j^{II}(\tau, \tau_2; \tau_3, \tau_1) \mathcal{G}_{j'}^{II}(\tau_3, \tau_1; \tau_2, \tau').$$

$$(27)$$

Again, in all cases except for the case of $G_{num}^{(3;c)}$, the 3! ways of choosing the three distinct hopping matrix elements involved completely cancels the $\frac{1}{3!}$ in the expansion. In the case of $G_{num}^{(3;c)}$, two of the hopping matrix elements are identical, so they can be chosen in only $\frac{3!}{2!}$ ways; hence there is a factor of $\frac{1}{2!}$ left uncanceled.

The restriction $(1 - \delta_{jj'})$ in the third-order contributions above is redundant except on nonbipartite lattices, such as nearest-neighbor hopping on a triangular lattice, or on a hypercubic lattice with second-neighbor hopping, where one can return to the starting site after three hops. In such cases, one has the additional term

$$G_{jj'}^{(3;d)}(\tau, \tau')_{num} = -\delta_{jj'} \sum_{j_2, j_1} (1 - \delta_{j_2 j})(1 - \delta_{jj_1}) t_{jj_2} t_{j_2 j_1} t_{j_1 j}$$

$$\times \int_{\tau_3} \int_{\tau_2} \int_{\tau_1} \mathcal{G}_j^{II}(\tau, \tau_1; \tau_3, \tau') \mathcal{G}_{j_2}(\tau_3, \tau_2)$$

$$\times \mathcal{G}_{j_1}(\tau_2, \tau_1). \qquad (28)$$

Note that in this term the constraints on j_1 and j_2 are actually redundant and can be omitted.

As in the second-order case, the above third-order terms can be recombined with the terms that arise as products of the first-order term from the numerator and the appropriate second-order terms from the denominator in Eq. (10) and re-expressed compactly in terms of the connected Green's functions $\mathfrak{G}^{(3)}$ and $\widetilde{\mathfrak{G}}^{(3)}$. One gets

$$G_{jj'}^{(3;0)}(\tau, \tau') = -\sum_{j_2, j_1} \mathfrak{G}_{jj_2 j_1 j'}^{(3)}(\tau, \tau'), \qquad (29)$$

$$G_{jj'}^{(3;1)}(\tau, \tau') = -\sum_{j_1} \widetilde{\mathfrak{G}}_{jj'j_1 j'}^{(3)}(\tau, \tau') - \sum_{j_2} \widetilde{\mathfrak{G}}_{jj_2 jj'}^{(3)}(\tau, \tau'),$$

$$(30)$$

$$G_{jj'}^{(3;2)}(\tau, \tau') = -\frac{1}{2!} \widetilde{\mathfrak{G}}_{jj'jj'}^{(3)}(\tau, \tau'). \qquad (31)$$

In nonbipartite cases, one has to add to this the additional contribution

$$G_{jj'}^{(3;3)}(\tau, \tau') = -\delta_{jj'} \sum_{j_2, j_1} \widetilde{\mathfrak{G}}_{jj_2 j_1 j}^{(3)}(\tau, \tau'). \qquad (32)$$

Note that in all the cases, use of the connected Green's functions allows one to avoid the clumsy restrictions on the intermediate sites that need to be summed over, and in addition, automatically includes the terms contributed by the denominator of Eq. (10). The diagrams that represent the above are shown in Figs. 1 and 2. The same results can also be derived using more formal methods, such as functional

integrals, generating functionals, and functional derivatives, but we do not go into such details here.

Next, we discuss the evaluation of the multiparticle single-site Green's functions at a site j as defined in Eqs. (12) and (13). The eigenstates of $\mathcal{H}_{0j}$ in Eq. (2) are also eigenstates of the number operator $\hat{n}_j$, and can hence be labeled by positive integers $n = 0, 1, \ldots$ corresponding to the number of bosons at site j, with energy eigenvalues which we label as $\epsilon_{j,n}$. One has

$$\mathcal{H}_{0j}|j,n\rangle = \epsilon_{j,n}|j,n\rangle, \quad \epsilon_{j,n} \equiv [V_T(\mathbf{r}_j) - \mu]n + \frac{U}{2}n(n-1). \tag{33}$$

The partition function of the jth site and the Boltzmann probability of occupancy of $|j,n\rangle$ in the thermal ensemble corresponding to $\mathcal{H}_{0j}$ are given, respectively, by

$$\mathcal{Z}_j = \sum_n \exp(-\beta\epsilon_{j,n}), \quad \rho_{j,n} = \exp(-\beta\epsilon_{j,n})/\mathcal{Z}_j. \tag{34}$$

It is convenient to define the ladder operators

$$\mathcal{X}_{j,n}^+ \equiv |j,n+1\rangle\langle j,n|, \quad \mathcal{X}_{j,n}^- \equiv |j,n-1\rangle\langle j,n|. \tag{35}$$

One can easily see that

$$a_j(\tau) = \sum_n e^{\tau\epsilon_{j,n}^-}\sqrt{n}\,\mathcal{X}_{j,n}^-, \quad a_j^\dagger(\tau) = \sum_n e^{\tau\epsilon_{j,n}^+}\sqrt{n+1}\,\mathcal{X}_{j,n}^+, \tag{36}$$

where

$$\epsilon_{j,n}^+ \equiv \epsilon_{j,(n+1)} - \epsilon_{j,n}, \quad \epsilon_{j,n}^- \equiv \epsilon_{j,(n-1)} - \epsilon_{j,n} \tag{37}$$

are the "particle" and "hole" "excitation energies" (with respect to the state with n bosons at site j) induced by the ladder operators $\mathcal{X}_{j,n_j}^+$ and $\mathcal{X}_{j,n_j}^-$, respectively.

Using the above, and the rather obvious rules for products of the ladder operators, it is easy to verify that for the one-particle Green's function, we have

$$\mathcal{G}_j(\tau_1, \tau_2) = \sum_n \rho_{j,n}[(n+1)e^{(\tau_2-\tau_1)\epsilon_{j,n}^+}\theta(\tau_1 - \tau_2)$$
$$+ ne^{(\tau_1-\tau_2)\epsilon_{j,n}^-}\theta(\tau_2 - \tau_1)]. \tag{38}$$

There is a compact way of working and writing this out which easily generalizes to n-particle Green's functions. Let $\mathbb{P}$ label the 2! possible permutations of (1,2), corresponding to $(1,2) \rightarrow (\mathbb{P}1, \mathbb{P}2)$, and $\mathcal{G}_j(\mathbb{P})$ denote $\mathcal{G}_j(\tau_1, \tau_2)$ in the domain $(\tau_{\mathbb{P}1} > \tau_{\mathbb{P}2})$. Furthermore, define $\sigma_1 \equiv -1$, $\sigma_2 \equiv +1$, $\epsilon_{j,n}^{\pm 1} \equiv \epsilon_{j,n}^{\pm}$, and $\mathcal{X}_{j,n}^{\pm 1} \equiv \mathcal{X}_{j,n}^{\pm}$. Then, one has

$$\mathcal{G}_j(\mathbb{P}) = \sum_n \rho_{j,n} \sum_{n_1,n_2} \langle j,n| \prod_{\ell=1,2}$$
$$\times \exp\left[\tau_{\mathbb{P}\ell}\epsilon_{j,n_\ell}^{\sigma_{\mathbb{P}\ell}}\right]\sqrt{n_\ell + \frac{1+\sigma_{\mathbb{P}\ell}}{2}}\mathcal{X}_{j,n_\ell}^{\sigma_{\mathbb{P}\ell}}|j,n\rangle$$
$$= \sum_n \rho_{j,n}\sqrt{n + \frac{1-\sigma_{\mathbb{P}1}}{2}}\sqrt{n + \frac{1+\sigma_{\mathbb{P}2}}{2}}$$
$$\times \exp[\tau_{\mathbb{P}2}\epsilon_{j,n}^{\sigma_{\mathbb{P}2}} - \tau_{\mathbb{P}1}\epsilon_{j,n}^{-\sigma_{\mathbb{P}1}}]. \tag{39}$$

As easily verified, for the identity permutation, corresponding to $\mathbb{P}1 = 1$, $\mathbb{P}2 = 2$, this reproduces the first term in Eq. (38). For the permutation corresponding to $\mathbb{P}1 = 2$, $\mathbb{P}2 = 1$, it reproduces the second term in Eq. (38).

Now, for the case of the two-particle Green's functions, let $\mathbb{P}$ label the 4! possible permutations of (1,2,3,4), corresponding to $(1,2,3,4) \rightarrow (\mathbb{P}1, \mathbb{P}2, \mathbb{P}3, \mathbb{P}4)$, and $\mathcal{G}_j^{II}(\mathbb{P})$ denote $\mathcal{G}_j^{II}(\tau_1, \tau_2; \tau_3, \tau_4)$ in the domain $(\tau_{\mathbb{P}1} > \tau_{\mathbb{P}2} > \tau_{\mathbb{P}3} > \tau_{\mathbb{P}4})$. For this case, we define $\sigma_1 = \sigma_2 \equiv -1$ and $\sigma_3 = \sigma_4 \equiv +1$. Using these definitions, we can show that

$$\mathcal{G}_j^{II}(\mathbb{P}) = \sum_n \rho_{j,n} \sum_{n_1,\ldots,n_4} \langle j,n| \prod_{\ell=1,\ldots,4}$$
$$\times \exp\left[\tau_{\mathbb{P}\ell}\epsilon_{j,n_\ell}^{\sigma_{\mathbb{P}\ell}}\right]\sqrt{n_\ell + \frac{1+\sigma_{\mathbb{P}\ell}}{2}}\mathcal{X}_{j,n_\ell}^{\sigma_{\mathbb{P}\ell}}|j,n\rangle$$
$$= \sum_n \rho_{j,n}\sqrt{n + \frac{1-\sigma_{\mathbb{P}1}}{2}}\sqrt{n - \sigma_{\mathbb{P}1} + \frac{1-\sigma_{\mathbb{P}2}}{2}}$$
$$\times \sqrt{n + \sigma_{\mathbb{P}4} + \frac{1+\sigma_{\mathbb{P}3}}{2}}\sqrt{n + \frac{1+\sigma_{\mathbb{P}4}}{2}}$$
$$\times \exp[\tau_{\mathbb{P}4}\epsilon_{j,n}^{\sigma_{\mathbb{P}4}} + \tau_{\mathbb{P}3}\epsilon_{j,n+\sigma_{\mathbb{P}4}}^{\sigma_{\mathbb{P}3}} - \tau_{\mathbb{P}2}\epsilon_{j,n-\sigma_{\mathbb{P}1}}^{-\sigma_{\mathbb{P}2}} - \tau_{\mathbb{P}1}\epsilon_{j,n}^{-\sigma_{\mathbb{P}1}}]. \tag{40}$$

For example, in the domain $(\tau_1 > \tau_2 > \tau_3 > \tau_4)$, corresponding to the identity permutation, this formula gives

$$\mathcal{G}_j^{II} = \langle a_j(\tau_1)a_j(\tau_2)a_j^\dagger(\tau_3)a_j^\dagger(\tau_4)\rangle_{\mathcal{H}_{0j}}$$
$$= \sum_n \rho_{j,n}(n+1)(n+2)\exp[(\tau_4 - \tau_1)\epsilon_{j,n}^+ + (\tau_3 - \tau_2)\epsilon_{j,n+1}^+]. \tag{41}$$

Using the above results, we can now readily compute the terms in the strong-coupling expansion of $C_{j'j}$ in Eq. (5) up to third order in the hopping amplitude. In the equations below, we denote $\mathfrak{C}_{j\cdots j'}^{(m)} \equiv \mathfrak{G}_{j\cdots j'}^{(m)}(0, 0^+)$, $\overline{\mathfrak{C}}_{j\cdots j'}^{(m)} = \overline{\mathfrak{G}}_{j\cdots j'}^{(m)}(0, 0^+)$, and $\widetilde{\mathfrak{G}}_{j\cdots j'}^{(m)} \equiv \widetilde{\mathfrak{G}}_{j\cdots j'}^{(m)}(0, 0^+)$.

The zeroth-order term is

$$C_{j'j}^{(0)} = -G_{jj'}^{(0)}(0, 0^+) = \delta_{j,j'}\langle\hat{n}_j\rangle_{\mathcal{H}_{0j}} = \delta_{j,j'}\sum_n n\rho_{j,n}. \tag{42}$$

The first-order term is

$$C_{j'j}^{(1)} = -G_{jj'}^{(1)}(0, 0^+) = \mathfrak{t}_{jj'}\int_{\tau_1}\mathcal{G}_j(0, \tau_1)\mathcal{G}_{j'}(\tau_1, 0^+) \equiv \mathfrak{C}_{jj'}^{(1)}. \tag{43}$$

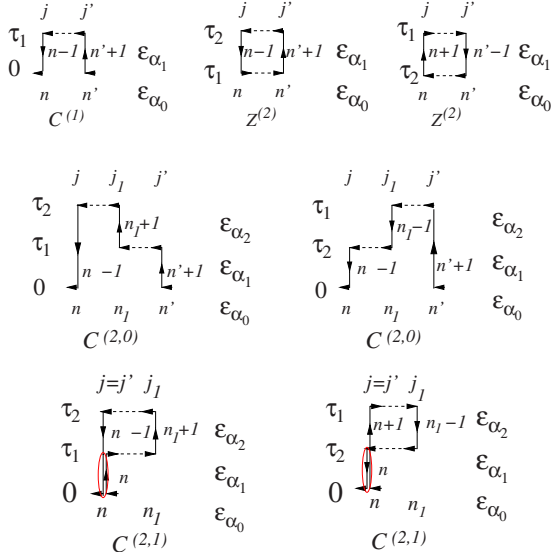The imaginary time integral is straightforward to evaluate. Using Eq. (38) or (39), we find

FIG. 3. (Color online) Strong-coupling diagrams for the correlation functions up to second order in t. The horizontal directed dashed lines indicate t between the sites labeled, and the vertical lines indicate single-site Green's functions $\mathcal{G}$. The ellipses (red online) at multiply visited sites denote the appearance of connected or cumulant Green's functions. Initial- and intermediate-state labels for the different possible imaginary time orderings shown are also indicated.

$$
\begin{aligned}
\mathfrak{C}_{jj'}^{(1)} &= \mathsf{t}_{jj'} \sum_{n,n'} n(n'+1)\rho_{j,n}\rho_{j',n'} \int_0^\beta d\tau_1 \exp[-\tau_1(\epsilon_{j,n}^- + \epsilon_{j',n'}^+)] \\
&= \mathsf{t}_{jj'} \sum_{n,n'} n(n'+1)\rho_{j,n}\rho_{j',n'} \left\{ \frac{1 - \exp[-\beta(\epsilon_{j,n}^- + \epsilon_{j',n'}^+)]}{\epsilon_{j,n}^- + \epsilon_{j',n'}^+} \right\} \\
&= \mathsf{t}_{jj'} \sum_{n,n'} n(n'+1) \left\{ \frac{\rho_{j,n}\rho_{j',n'}}{\epsilon_{j,n}^- + \epsilon_{j',n'}^+} + \frac{\rho_{j,n-1}\rho_{j',n'+1}}{\epsilon_{j,n-1}^+ + \epsilon_{j',n'+1}^-} \right\} \\
&= \mathsf{t}_{jj'} \sum_{n,n'} \rho_{j,n}\rho_{j',n'} \left\{ \frac{n(n'+1)}{\epsilon_{j,n}^- + \epsilon_{j',n'}^+} + \frac{(n+1)n'}{\epsilon_{j,n}^+ + \epsilon_{j',n'}^-} \right\}. \quad (44)
\end{aligned}
$$

This can be represented by the diagram labeled $C^{(1)}$ in Fig. 3. The third line of Eq. (44) is written in a form that can be directly constructed from this diagram in a way that is immediately generalizable to higher order (see below). The fourth line contains a second form of the same result, obtained by relabeling the bosonic occupation numbers in the second term of the third line in a way that makes the zero-temperature limit obvious.

There are two second-order terms in $C_{j'j}$ corresponding to the two terms in $G_{jj'}$ [Eqs. (21) and (23)].

$$
C_{j'j}^{(2,0)} = -G_{jj'}^{(2;0)}(0,0^+) = -\sum_{j_1} \mathfrak{C}_{jj_1j'}^{(2)}, \quad (45)
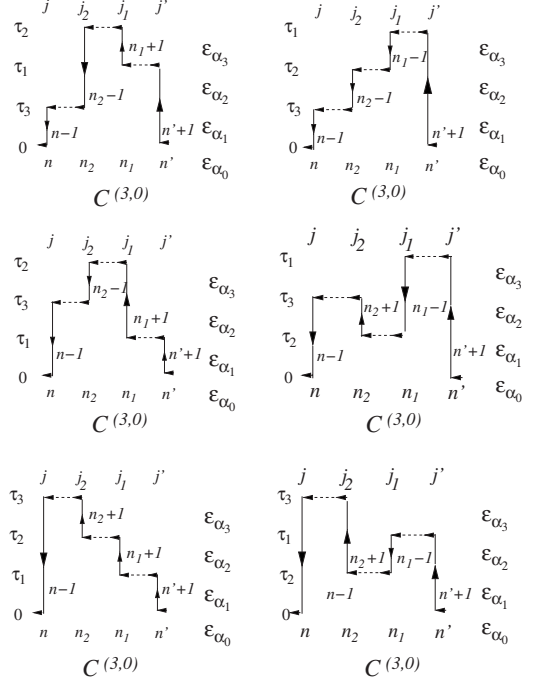$$

and

FIG. 4. Strong-coupling diagrams for the correlation functions $C^{(3,0)}$. The horizontal directed dashed lines indicate the hopping matrix t between the sites labeled, and the vertical lines indicate single-site Green's functions $\mathcal{G}$. There are no multiply visited sites in these diagrams. Initial- and intermediate-state labels for the different possible imaginary time orderings shown are also indicated.

$$
\begin{aligned}
C_{j'j}^{(2,1)} &= -G_{jj'}^{(2;1)}(0,0^+) \\
&= -\delta_{jj'} \sum_{j_1} \widetilde{\mathfrak{C}}_{jj_1j}^{(2)} \\
&= -\delta_{jj'} \sum_{j_1} \{\overline{\mathfrak{C}}_{jj_1j}^{(2)} - [\mathfrak{C}_{jj_1j'}^{(2)}]_{j'=j} - \langle \hat{n}_j \rangle_{\mathcal{H}_{0j}} \mathcal{Z}_{jj_1}^{(2)} \}. \quad (46)
\end{aligned}
$$

Similarly, one obtains the various terms contributing to $C_{j'j}$ in third order, which we label $C_{j'j}^{(3,0)}, C_{j'j}^{(3,1)}, \ldots$, by setting $\tau = 0$ and $\tau' = 0^+$ in Eq. (29), Eq. (30), and so on. One finds

$$
C_{j'j}^{(3,0)} = \sum_{j_2,j_1} \mathfrak{C}_{jj_2j_1j'}^{(3)}, \quad (47)
$$

$$
\begin{aligned}
C_{j'j}^{(3,1)} &= \sum_{j_1} \widetilde{\mathfrak{C}}_{jj'j_1j'}^{(3)} + \sum_{j_2} \widetilde{\mathfrak{G}}_{jj_2jj'}^{(3)} \\
&= \sum_{j_1} \{\overline{\mathfrak{C}}_{jj'j_1j'}^{(3)} - \mathfrak{C}_{jj'j_1j'}^{(3)} - \mathfrak{C}_{jj'}^{(1)} \mathcal{Z}_{j'j_1}^{(2)}\} \\
&\quad + \sum_{j_2} \{\overline{\mathfrak{C}}_{jj_2jj'}^{(3)} - \mathfrak{C}_{jj_2jj'}^{(3)} - \mathfrak{C}_{jj'}^{(1)} \mathcal{Z}_{j_2j}^{(2)}\}, \quad (48)
\end{aligned}
$$

$$
\begin{aligned}
C_{j'j}^{(3,2)} &= \frac{1}{2!}\widetilde{\mathfrak{C}}_{jj'jj'}^{(3)} = \frac{1}{2!}\{\overline{\mathfrak{C}}_{jj'jj'}^{(3)} - 2[\overline{\mathfrak{C}}_{jj'j_1j'}^{(3)}]_{j_1=j} - 2[\overline{\mathfrak{C}}_{jj_2jj'}^{(3)}]_{j_2=j'} \\
&\quad + 2\mathfrak{C}_{jj'jj'}^{(3)} + 2\mathfrak{C}_{jj'}^{(1)} \mathcal{Z}_{j'j}^{(2)}\}. \quad (49)
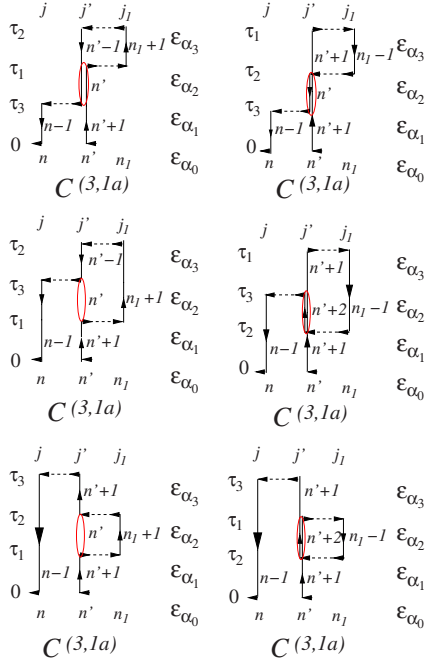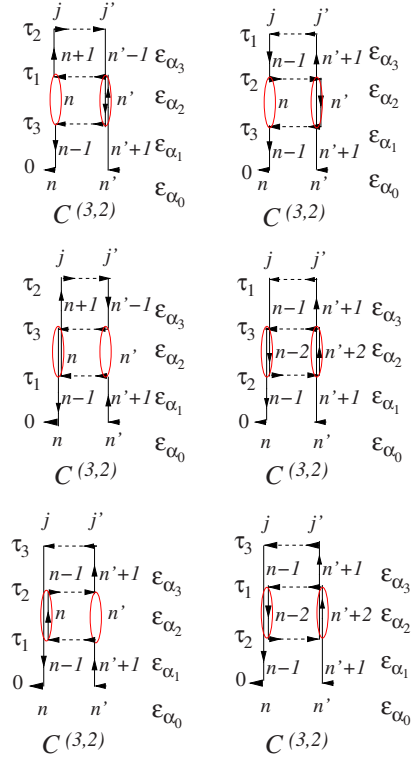\end{aligned}
$$

FIG. 5. (Color online) Strong-coupling diagrams for the correlation functions $C^{(3,1)}$. The horizontal directed dashed lines indicate the hopping matrix t between the sites labeled, and the vertical lines indicate single-site Green's functions $\mathcal{G}$. The one ellipse (red online); at multiply visited sites denotes the appearance of connected or cumulant Green's functions. Initial- and intermediate-state labels for the different possible imaginary time orderings shown are also indicated.

The imaginary time integrals that appear in these expressions are most conveniently evaluated by splitting them up into separate integrals corresponding to each of the different $(m!)$ imaginary time orderings of imaginary time integration variables (in mth order). With each such imaginary time-ordered term one can associate a unique diagram, as shown in Figs. 3–6 up to third order. The diagrams are labeled by the sites that appear, the "initial" (equals the "final") and the "intermediate states" at these sites as determined by the boson occupation numbers at these sites in each of the imaginary time intervals, whose labeling corresponds to the boson creation and destruction processes at the sites. (The boson occupation numbers at the sites that do not appear in a diagram do not change with imaginary time, and play a spectator role, and hence do not appear in the contributions to $C_{j'j}$.) The "matrix elements" that are associated with these processes are then uniquely determined and can be written down by inspection from the labeling. For such a diagram of mth order, let $\mathcal{E}_{\alpha_0}$ and $\mathcal{E}_{\alpha_1}, \ldots, \mathcal{E}_{\alpha_m}$ denote the energy eigenvalues of $\mathcal{H}_0$ for the initial (or final) state and the m intermediate states, respectively. Then the imaginary time integral is of the form

$$I_m(\beta; \mathcal{E}_{\alpha_m}, \ldots, \mathcal{E}_{\alpha_1}, \mathcal{E}_{\alpha_0}) = \frac{e^{-\beta\mathcal{E}_{\alpha_0}}}{\mathcal{Z}} \int_0^\beta d\tau_m \int_0^{\tau_m} d\tau_{m-1} \cdots \int_0^{\tau_2}$$
$$\times d\tau_1 e^{[\tau_m(\mathcal{E}_{\alpha_0} - \mathcal{E}_{\alpha_m}) + \tau_{m-1}(\mathcal{E}_{\alpha_m} - \mathcal{E}_{\alpha_{m-1}}) + \cdots + \tau_2(\mathcal{E}_{\alpha_3} - \mathcal{E}_{\alpha_2}) + \tau_1(\mathcal{E}_{\alpha_2} - \mathcal{E}_{\alpha_1})]}.$$
$$(50)$$

FIG. 6. (Color online) Strong-coupling diagrams for the correlation functions $C^{(3,2)}$. The horizontal directed dashed lines indicate the hopping matrix element t between the sites labeled, and the vertical lines indicate single-site Green's functions $\mathcal{G}$. The two ellipses (red online) at multiply visited sites denote the appearance of connected or cumulant Green's functions. Initial- and intermediate-state labels for the different possible imaginary time orderings shown are also indicated.

This is easily evaluated using Laplace-transform techniques, as shown in Appendix A. If the energies are all distinct, then one finds that the integral is the following sum of $m+1$ terms:

$$I_m(\beta; \mathcal{E}_{\alpha_m}, \ldots, \mathcal{E}_{\alpha_1}, \mathcal{E}_{\alpha_0}) = \sum_{\ell=0}^m \frac{e^{-\beta\mathcal{E}_{\alpha_\ell}}}{\mathcal{Z}} \prod_{\ell' \neq \ell} \frac{1}{(\mathcal{E}_{\alpha_{\ell'}} - \mathcal{E}_{\alpha_\ell})}. \quad (51)$$

Note that only energy differences appear in the energy denominators in this expression, and they are related in a simple way to the boson creation and destruction processes at the sites that appear in the diagrams. These can be written down by inspection from the labeling shown in each diagram. As the initial and intermediate states at all the sites that do not appear in the diagrams are constrained to be the same, one can replace the Boltzmann factors for the initial and intermediate states by a product of the density matrices *for just the sites that appear in the diagrams*.

The expression in Eq. (51) is nonsingular and remains well defined even when one or more of the energies $\mathcal{E}_{\alpha_0}, \mathcal{E}_{\alpha_1}, \ldots, \mathcal{E}_{\alpha_m}$ become equal, as clearly happens, for example, in the diagrams for $C^{(2,1)}$ (see Fig. 3). For example, if one and only one pair of energies are equal, say, $\mathcal{E}_{\alpha_r} = \mathcal{E}_{\alpha_p}$, then instead of Eq. (51) one should use the expression

$$\sum_{\ell \neq r,p} \frac{e^{-\beta \mathcal{E}_{\alpha_\ell}}}{\mathcal{Z}} \prod_{\ell' \neq \ell} \frac{1}{(\mathcal{E}_{\alpha_{\ell'}} - \mathcal{E}_{\alpha_\ell})} + \frac{e^{-\beta \mathcal{E}_{\alpha_r}}}{\mathcal{Z}} \left[\beta - \sum_{\ell \neq r,p} \frac{1}{(\mathcal{E}_{\alpha_\ell} - \mathcal{E}_{\alpha_r})} \right] \prod_{\ell' \neq r,p} \frac{1}{(\mathcal{E}_{\alpha_{\ell'}} - \mathcal{E}_{\alpha_r})}, \tag{52}$$

which it reduces to in this limit (see Appendix A for further details).

Figure 3 shows the two diagrams for $\mathfrak{C}^{(2)}_{jj_1j'}$ [labeled $C^{(2,0)}$], corresponding to the two imaginary time orderings $\tau_2 > \tau_1$ and $\tau_1 > \tau_2$. Each diagram gives rise to three contributions as pointed out above, which are easily written down using the above rules, leading to

$$\mathfrak{C}^{(2)}_{jj_1j'} = t_{jj_1} t_{j_1j'} \sum_{n,n_1,n'} \left\{ n(n_1+1)(n'+1) \left[\frac{\rho_{j,n}\rho_{j_1,n_1}\rho_{j',n'}}{(\epsilon^-_{j,n} + \epsilon^+_{j_1,n_1})(\epsilon^-_{j,n} + \epsilon^+_{j',n'})} + \frac{\rho_{j,n-1}\rho_{j_1,n_1}\rho_{j',n'+1}}{(\epsilon^+_{j,n-1} + \epsilon^-_{j',n'+1})(\epsilon^+_{j_1,n_1} + \epsilon^-_{j',n'+1})} \right. \right.$$
$$\left. + \frac{\rho_{j,n-1}\rho_{j_1,n_1+1}\rho_{j',n'}}{(\epsilon^+_{j,n-1} + \epsilon^-_{j_1,n_1+1})(\epsilon^-_{j_1,n_1+1} + \epsilon^+_{j',n'})} \right] + nn_1(n'+1)$$
$$\left. \times \left[\frac{\rho_{j,n}\rho_{j_1,n_1}\rho_{j',n'}}{(\epsilon^-_{j,n} + \epsilon^+_{j',n'})(\epsilon^+_{j_1,n_1} + \epsilon^-_{j',n'})} + \frac{\rho_{j,n-1}\rho_{j_1,n_1}\rho_{j',n'+1}}{(\epsilon^+_{j,n-1} + \epsilon^-_{j_1,n_1})(\epsilon^+_{j,n-1} + \epsilon^-_{j',n'+1})} + \frac{\rho_{j,n}\rho_{j_1,n_1-1}\rho_{j',n'+1}}{(\epsilon^-_{j,n} + \epsilon^+_{j_1,n_1-1})(\epsilon^+_{j_1,n_1-1} + \epsilon^-_{j',n'+1})} \right] \right\} \tag{53}$$

$$= t_{jj_1} t_{j_1j'} \sum_{n,n_1,n'} \rho_{j,n}\rho_{j_1,n_1}\rho_{j',n'} \left\{ \left[\frac{n(n_1+1)(n'+1)}{(\epsilon^-_{j,n} + \epsilon^+_{j_1,n_1})(\epsilon^-_{j,n} + \epsilon^+_{j',n'_j})} + \frac{(n+1)(n_1+1)n'}{(\epsilon^+_{j,n} + \epsilon^-_{j',n'})(\epsilon^+_{j_1,n_1} + \epsilon^-_{j',n'})} + \frac{(n+1)n_1(n'+1)}{(\epsilon^+_{j,n} + \epsilon^-_{j_1,n_1})(\epsilon^-_{j_1,n_1} + \epsilon^+_{j',n'})} \right] \right.$$
$$\left. + \left[\frac{nn_1(n'+1)}{(\epsilon^-_{j,n} + \epsilon^+_{j',n'})(\epsilon^-_{j,n_1} + \epsilon^+_{j',n'})} + \frac{(n+1)n_1n'}{(\epsilon^+_{j,n} + \epsilon^-_{j_1,n_1})(\epsilon^+_{j,n} + \epsilon^-_{j',n'})} + \frac{n(n_1+1)n'}{(\epsilon^-_{j,n} + \epsilon^+_{j_1,n_1})(\epsilon^+_{j_1,n_1} + \epsilon^-_{j',n'})} \right] \right\}. \tag{54}$$

Again, the second form of the result [Eq. (54)] is obtained by appropriately relabeling the bosonic occupation numbers in four of the six terms in the first form [Eq. (53)], and is easier to use at $T=0$.

Similarly, from the diagrams contributing to $\overline{\mathfrak{C}}^{(2)}_{jj_1j}$ (labeled $C^{(2,1)}$) and $\mathcal{Z}^{(2)}_{jj_1}$ (labeled $Z^{(2)}$) shown in Fig. 3, and using Eq. (52), we obtain, for the two equivalent forms for each,

$$\overline{\mathfrak{C}}^{(2)}_{jj_1j} = t_{jj_1} t_{j_1j} \sum_{n,n_1} (n) \left\{ n(n_1+1) \left[\frac{\rho_{j,n}\rho_{j_1,n_1}}{(\epsilon^-_{j,n} + \epsilon^+_{j_1,n_1})} \left(\beta - \frac{1}{(\epsilon^-_{j,n} + \epsilon^+_{j_1,n_1})} \right) + \frac{\rho_{j,n-1}\rho_{j_1,n_1+1}}{(\epsilon^+_{j,n-1} + \epsilon^-_{j_1,n_1+1})^2} \right] \right.$$
$$\left. + (n+1)n_1 \left[\frac{\rho_{j,n}\rho_{j_1,n_1}}{(\epsilon^+_{j,n} + \epsilon^-_{j_1,n_1})} \left(\beta - \frac{1}{(\epsilon^+_{j,n} + \epsilon^-_{j_1,n_1})} \right) + \frac{\rho_{j,n+1}\rho_{j_1,n_1-1}}{(\epsilon^+_{j,n+1} + \epsilon^+_{j_1,n_1-1})^2} \right] \right\} \tag{55}$$

$$= t_{jj_1} t_{j_1j} \sum_{n,n_1} \rho_{j,n}\rho_{j_1,n_1} \left\{ \left[\frac{n(n_1+1)n}{(\epsilon^-_{j,n} + \epsilon^+_{j_1,n_1})} \left(\beta - \frac{1}{(\epsilon^-_{j,n} + \epsilon^+_{j_1,n_1})} \right) + \frac{(n+1)n_1(n+1)}{(\epsilon^+_{j,n} + \epsilon^-_{j_1,n_1})^2} \right] \right.$$
$$\left. + \left[\frac{(n+1)n_1n}{(\epsilon^+_{j,n} + \epsilon^-_{j_1,n_1})} \left(\beta - \frac{1}{(\epsilon^+_{j,n} + \epsilon^-_{j_1,n_1})} \right) + \frac{n(n_1+1)(n-1)}{(\epsilon^-_{j,n} + \epsilon^+_{j_1,n_1})^2} \right] \right\}, \tag{56}$$

$$\mathcal{Z}^{(2)}_{jj_1} = t_{jj_1} t_{j_1j} \sum_{n,n_1} \left\{ n(n_1+1) \left[\frac{\rho_{j,n}\rho_{j_1,n_1}}{(\epsilon^-_{j,n} + \epsilon^+_{j_1,n_1})} \left(\beta - \frac{1}{(\epsilon^-_{j,n} + \epsilon^+_{j_1,n_1})} \right) + \frac{\rho_{j,n-1}\rho_{j_1,n_1+1}}{(\epsilon^+_{j,n-1} + \epsilon^-_{j_1,n_1+1})^2} \right] \right.$$
$$\left. + (n+1)n_1 \left[\frac{\rho_{j,n}\rho_{j_1,n_1}}{(\epsilon^+_{j,n} + \epsilon^-_{j_1,n_1})} \left(\beta - \frac{1}{(\epsilon^+_{j,n} + \epsilon^-_{j_1,n_1})} \right) + \frac{\rho_{j,n+1}\rho_{j_1,n_1-1}}{(\epsilon^-_{j,n+1} + \epsilon^+_{j_1,n_1-1})^2} \right] \right\} \tag{57}$$

$$= t_{jj_1} t_{j_1j} \sum_{n,n_1} \rho_{j,n}\rho_{j_1,n_1} \times \left\{ \left[\frac{n(n_1+1)}{(\epsilon^-_{j,n} + \epsilon^+_{j_1,n_1})} \left(\beta - \frac{1}{(\epsilon^-_{j,n} + \epsilon^+_{j_1,n_1})} \right) + \frac{(n+1)n_1}{(\epsilon^+_{j,n} + \epsilon^-_{j_1,n_1})^2} \right] \right.$$
$$\left. + \left[\frac{(n+1)n_1}{(\epsilon^+_{j,n} + \epsilon^-_{j_1,n_1})} \left(\beta - \frac{1}{(\epsilon^+_{j,n} + \epsilon^-_{j_1,n_1})} \right) + \frac{n(n_1+1)}{(\epsilon^-_{j,n} + \epsilon^+_{j_1,n_1})^2} \right] \right\}. \tag{58}$$

Simplifying these expressions we find

$$\overline{\mathfrak{C}}^{(2)}_{jj_1j} = \mathsf{t}_{jj_1}\mathsf{t}_{j_1j}\sum_{n,n_1}\rho_{j,n}\rho_{j_1,n_1}\left\{\beta n\left[\frac{n(n_1+1)}{(\epsilon^-_{j,n}+\epsilon^+_{j_1,n_1})}+\frac{(n+1)n_1}{(\epsilon^+_{j,n}+\epsilon^-_{j_1,n_1})}\right]\right.$$
$$\left.+\left[\frac{(n+1)n_1}{(\epsilon^+_{j,n}+\epsilon^-_{j_1,n_1})^2}-\frac{n(n_1+1)}{(\epsilon^-_{j,n}+\epsilon^+_{j_1,n_1})^2}\right]\right\}, \quad (59)$$

$$\mathcal{Z}^{(2)}_{jj_1} = \mathsf{t}_{jj_1}\mathsf{t}_{j_1j}\sum_{n,n_1}\rho_{j,n}\rho_{j_1,n_1}\left\{\beta\left[\frac{n(n_1+1)}{(\epsilon^-_{j,n}+\epsilon^+_{j_1,n_1})}+\frac{(n+1)n_1}{(\epsilon^+_{j,n}+\epsilon^-_{j_1,n_1})}\right]\right\}. \quad (60)$$

Finally, Figs. 4–6 show the diagrams corresponding, respectively, to $\mathfrak{C}^{(3)}_{jj_2j_1j'}$, $\overline{\mathfrak{C}}^{(3)}_{jj'j_1j'}$ (the diagrams for $\overline{\mathfrak{C}}^{(3)}_{jj_2jj'}$ can be obtained from those in Fig. 5 by symmetry and a simple relabeling), and $\overline{\mathfrak{C}}^{(3)}_{jj'jj'}$. (For simplicity, since we do not discuss nonbipartite lattices in detail in this paper; the diagrams for $\overline{\mathfrak{C}}^{(3)}_{jj_2j_1j}$ are not shown.) In each case, there are six possible orderings of the imaginary time variables τ_3, τ_2, and τ_1 [listed in the order $(\tau_3>\tau_2>\tau_1)$, $(\tau_2>\tau_3>\tau_1)$, $(\tau_2>\tau_1>\tau_2)$, $(\tau_3>\tau_1>\tau_2)$, $(\tau_1>\tau_3>\tau_2)$, and $(\tau_1>\tau_2>\tau_3)$ below]. From each imaginary time ordering we get four contributions corresponding to the initial and three intermediate states (apart from the subtractions arising from the connected two-particle Green's functions). The contributions can be written down straightforwardly using the rules stated above, and we present them in Appendix B.

It is easy to see that the methods we have discussed above permit one, in principle, to similarly write down the contributions to $G_{jj'}$ and $C_{j'j}$ to higher orders as well, though the calculations will become increasingly tedious *unless one can find a way to automate them.* However, it is possible to calculate sums of subsets of these contributions to arbitrary orders.

The easiest subset to sum is $G^{(m,0)}_{jj'}$, with contributions coming entirely from "self-avoiding lattice walks" while computing thermal averages, and therefore involving only single-particle single-site Green's functions, *but ignoring the self-avoidance constraint while summing over the different possible walks.* From the above analysis it is clear that the resulting term is

$$G^{(m;0)}_{jj'}(\tau,\tau') = (-1)^{(m+1)}\mathsf{t}_{jj_{m-1}}\mathsf{t}_{j_{m-1}j_{m-1}}\cdots\mathsf{t}_{j_2j_1}\mathsf{t}_{j_1j'}$$
$$\times\int_{\tau_m}\int_{\tau_{m-1}}\cdots\int_{\tau_2}\int_{\tau_1}\mathcal{G}_j(\tau,\tau_m)$$
$$\times\mathcal{G}_{j_{m-1}}(\tau_m,\tau_{m-1})\cdots\mathcal{G}_{j_1}(\tau_2,\tau_1)\mathcal{G}_{j'}(\tau_1,\tau'). \quad (61)$$

The sum of these to arbitrary order, together with $G^{(1)}_{jj'}$ [Eq. (15)] and $G^{(0)}_{jj'}$ [Eq. (14)], corresponds to a geometric series for the Green's function regarded as a matrix (denoted by boldface letters and/or square brackets below) with lattice sites and imaginary times as indices, and corresponds to the well-known RPA result,

$$[\mathbf{G}^{RPA}]^{-1}_{jj'}(\tau,\tau') = [\mathcal{G}_j]^{-1}(\tau,\tau')\delta_{jj'}+\delta(\tau,\tau')\mathsf{t}_{jj'}. \quad (62)$$

By taking a Fourier transform with respect to the even Matsubara frequencies $i\Omega_m\equiv 2m\pi k_BT$, with $m=0,\pm 1,\pm 2,\ldots$, one can write this as a matrix equation involving only lattice indices:

$$[\mathbf{G}^{RPA}]^{-1}_{jj'}(i\Omega_m) = [\mathcal{G}_j(i\Omega_m)]^{-1}\delta_{jj'}+\mathsf{t}_{jj'}, \quad (63)$$

where from Eq. (38), the single-site Green's function at a fixed frequency is easily obtained as

$$\mathcal{G}_j(i\Omega_m) = \sum_n \rho_{j,n}\left[\frac{n+1}{i\Omega_m-\epsilon^+_{j,n}}-\frac{n}{i\Omega_m+\epsilon^-_{j,n}}\right]. \quad (64)$$

The RPA correlation function can then be straightforwardly obtained, in view of Eq. (5), as the Matsubara frequency sum

$$C_{j'j} = -[\mathbf{G}]_{jj'}(0,0^+) = -\sum_{\Omega_m}G_{jj'}(i\Omega_m)e^{i\Omega_m0^+}, \quad (65)$$

by using $[\mathbf{G}^{RPA}]$ for $[\mathbf{G}]$. While the frequency sum can in principle be evaluated using standard contour integral techniques [29], in the inhomogeneous case the above calculation involves a matrix inversion with respect to the site indices.

The calculations simplify, however, for the case of a homogeneous system, i.e., without a trap or disorder potential, and for $T\to 0$. Then all the sites are identical, and in a generic case, the ground state of $\mathcal{H}_{0j}$ at every site corresponds to the same fixed boson occupancy, which we denote n. In this limit, one has $\epsilon_n=-\mu n+\frac{U}{2}n(n-1)$, whence $\epsilon^+_n=-\mu+Un$ and $\epsilon^-_n=\mu-U(n-1)$. The RPA momentum distribution can be calculated exactly analytically in this case, as discussed in detail by Sengupta and Dupuis [22]. From Eq. (64), at $T\ll\epsilon^\pm_n$ we get, for all sites j,

$$\mathcal{G}_j(i\Omega_m) = \left[\frac{n+1}{i\Omega_m-\epsilon^+_n}-\frac{n}{i\Omega_m+\epsilon^-_n}\right]. \quad (66)$$

Hence,

$$[\mathbf{G}^{RPA}]_{\mathbf{k}}(i\Omega_m) = \frac{1}{[\mathcal{G}_j(i\Omega_m)]^{-1}-\epsilon_{\mathbf{k}}} = \frac{1-z_{\mathbf{k}}}{i\Omega_m-E^-_{\mathbf{k}}}+\frac{z_{\mathbf{k}}}{i\Omega_m-E^+_{\mathbf{k}}}, \quad (67)$$

with poles at $E^\pm_{\mathbf{k}}\equiv[\epsilon_{\mathbf{k}}+\epsilon^+_n-\epsilon^-_n\pm\sqrt{\epsilon^2_{\mathbf{k}}+2\epsilon_{\mathbf{k}}U(2n+1)+U^2}]/2$ and residues determined in terms of $z_{\mathbf{k}}\equiv(E^+_{\mathbf{k}}+\mu+U)/(E^+_{\mathbf{k}}-E^-_{\mathbf{k}})$. The RPA momentum distribution at $T=0$ is just the negative of the spectral weight of the pole at $E^-_{\mathbf{k}}$; i.e.,

$$n^{RPA}_{\mathbf{k}} = z_{\mathbf{k}}-1 = \frac{E^-_{\mathbf{k}}+\mu+U}{\sqrt{\epsilon^2_{\mathbf{k}}+2\epsilon_{\mathbf{k}}U(2n+1)+U^2}}. \quad (68)$$

The challenge, of course, is to go beyond the RPA. One way to achieve this, by summing further infinite subsets of contributions to $G_{jj'}$ beyond the RPA, is by using the Dyson equation [compare Eq. (62)],

$$[\mathbf{G}]^{-1}_{jj'}(\tau,\tau') = [\mathcal{G}_j]^{-1}(\tau,\tau')\delta_{jj'}+\delta(\tau,\tau')\mathsf{t}_{jj'}-\mathbf{\Sigma}^{(2)}_{jj'}(\tau,\tau')-\mathbf{\Sigma}^{(3)}_{jj'}$$
$$\times(\tau,\tau')-\cdots, \quad (69)$$

where $\mathbf{\Sigma}^{(m)}$ denotes a self-energy correction that corrects the

RPA to order t^m. By re-expanding the inverse of this equation and comparing with the expansion for $G_{jj'}$ discussed earlier, it is straightforward to obtain the following expressions for the self-energy corrections up to third order in t:

$$\Sigma_{jj'}^{(2)}(\tau,\tau') = \int_{\tau_2}\int_{\tau_1} [\mathcal{G}_j]^{-1}(\tau,\tau_2) G_{jj'}^{(2;1)}(\tau_2,\tau_1)[\mathcal{G}_{j'}]^{-1}(\tau_1,\tau')$$

$$= \delta_{jj'}\int_{\tau_2}\int_{\tau_1}\sum_{j_1} [\mathcal{G}_j]^{-1}(\tau,\tau_2) \widetilde{\mathfrak{G}}_{jj_1j}^{(2)}(\tau_2,\tau_1)$$
$$\times [\mathcal{G}_j]^{-1}(\tau_1,\tau'), \tag{70}$$

with $\widetilde{\mathfrak{G}}^{(2)}$ as given in Eq. (23). Similarly,

$$\Sigma_{jj'}^{(3)}(\tau,\tau') = \int_{\tau_2}\int_{\tau_1} [\mathcal{G}_j]^{-1}(\tau,\tau_2)[G_{jj'}^{(3;1)}(\tau_2,\tau_1) + G_{jj'}^{(3;2)}(\tau_2,\tau_1)$$
$$+ G_{jj'}^{(3;3)}(\tau_2,\tau_1)][\mathcal{G}_{j'}]^{-1}(\tau_1,\tau')$$
$$+ \int_{\tau_1}\sum_{j_2} t_{jj_2} G_{j_2j'}^{(2;1)}(\tau,\tau_1)[\mathcal{G}_{j'}]^{-1}(\tau_1,\tau')$$
$$+ \int_{\tau_2}\sum_{j_2} [\mathcal{G}_j]^{-1}(\tau,\tau_2) G_{jj_2}^{(2;1)}(\tau_2,\tau') t_{j_2j'}. \tag{71}$$

It is straightforward to verify using the expressions given in Eqs. (23) and (30)–(32), that the term involving $G_{jj'}^{(3;1)}$ exactly cancels the two terms involving $G_{jj'}^{(2;1)}$ above, and one obtains

$$\Sigma_{jj'}^{(3)}(\tau,\tau') = -\int_{\tau_2}\int_{\tau_1} [\mathcal{G}_j]^{-1}(\tau,\tau_2)\left[\frac{1}{2!}\widetilde{\mathfrak{G}}_{jj'jj}^{(3)}(\tau_2,\tau_1)\right.$$
$$\left. + \delta_{jj'}\sum_{j_2,j_1}\widetilde{\mathfrak{G}}_{jj_2j_1j}^{(3)}(\tau_2,\tau_1)\right][\mathcal{G}_{j'}]^{-1}(\tau_1,\tau'). \tag{72}$$

One can in principle evaluate these expressions for the self-energies explicitly using the techniques discussed above, and thereby determine spectral functions as well as the momentum distribution function using Eq. (65). We plan to complete such work in the future.

However, in this paper we adopt a different procedure for calculating the momentum distribution function for the homogeneous case and in the $T \to 0$ limit. We directly evaluate the expressions for $C_{j'j}$ up to third order in t. Then we use a scaling ansatz for the momentum distribution function determined in such a way that when expanded in powers of t, it agrees with our calculated results, thereby effecting an infinite-order resummation in a different way which automatically has the correct critical behavior at the Mott insulator-to-superfluid transition.

The direct evaluation of our expressions for $C_{j'j}$ in the homogeneous $T \to 0$ limit is straightforward. The $T \to 0$ limit is easiest to implement using *the second form of these expressions*, where, just as discussed above in case of the RPA, for $T \ll \epsilon_n^{\pm}$ the sums over the initial and intermediate states are all restricted to n. The excitation energies that occur in the energy denominators in these expressions are given by

$\epsilon_n^+ + \epsilon_n^- = U$, $\epsilon_n^+ + \epsilon_{n-1}^- + \epsilon_n^+ + \epsilon_n^- = \epsilon_n^+ + \epsilon_n^- + \epsilon_{n+1}^+ + \epsilon_n^- = 3U$, and $\epsilon_n^+ + \epsilon_{n-1}^- + \epsilon_{n+1}^+ + \epsilon_n^- = 4U$. Hence, we find

$$C_{j'j}^{(0)} = \delta_{j,j'} n, \tag{73}$$

$$C_{j'j}^{(1)} = \mathfrak{C}_{jj'}^{(1)} = t_{jj'}\left\{\frac{2n(n+1)}{U}\right\}. \tag{74}$$

For the second-order terms we obtain

$$\mathfrak{C}_{jj_1j'}^{(2)} = t_{jj_1}t_{j_1j'}\left\{\left[\frac{3n(n+1)^2}{U^2}\right] + \left[\frac{3n^2(n+1)}{U^2}\right]\right\}$$
$$= t_{jj_1}t_{j_1j'}\left\{\frac{3n(n+1)(2n+1)}{U^2}\right\}, \tag{75}$$

$$\overline{\mathfrak{C}}_{jj_1j}^{(2)} = n\mathcal{Z}_{jj_1}^{(2)} = n\beta t_{jj_1}t_{j_1j}\left\{\frac{2n(n+1)}{U}\right\}. \tag{76}$$

Hence, using Eqs. (45) and (46), we find

$$C_{j'j}^{(2,0)} = -\left[\sum_{j_1} t_{jj_1}t_{j_1j'}\right]\left\{\frac{3n(n+1)(2n+1)}{U^2}\right\}, \tag{77}$$

$$C_{j'j}^{(2,1)} = -\delta_{j,j'}C_{jj}^{(2,0)}. \tag{78}$$

Note that in $C^{(2,1)}$ the (divergent) temperature-dependent terms from $\overline{\mathfrak{C}}^{(2)}$ and $\mathcal{Z}^{(2)}$ exactly cancel, as they ought to.

Finally, we consider the various third-order terms. We get the following results:

$$\mathfrak{C}_{jj_2j_1j'}^{(3)} = t_{jj_2}t_{j_2j_1}t_{j_1j'}\left\{\left[\frac{4n(n+1)^3}{U^3}\right] + 4\left[\frac{3n^2(n+1)^2}{U^3}\right]\right.$$
$$\left. + \left[\frac{4n^3(n+1)}{U^3}\right]\right\} \tag{79}$$

$$= t_{jj_2}t_{j_2j_1}t_{j_1j'}\left\{\frac{4n(n+1)(5n^2+5n+1)}{U^3}\right\}, \tag{80}$$

whence

$$C_{j'j}^{(3,0)} = \left[\sum_{j_2,j_1} t_{jj_2}t_{j_2j_1}t_{j_1j'}\right]\left\{\frac{4n(n+1)(5n^2+5n+1)}{U^3}\right\}. \tag{81}$$

Furthermore,

$$\overline{\mathfrak{C}}_{jj'j_1j'}^{(3)} = t_{jj'}t_{j'j_1}t_{j_1j'}\left\{\left[\frac{2n(n+1)^3}{U^3} + \frac{n^2(n+1)^2}{U^3}(\beta U - 2)\right]\right.$$
$$+ 2\left[\frac{2n^2(n+1)^2}{U^3} + \frac{n(n+1)(n^2-1)}{3U^3}\right.$$
$$\left. + \frac{n(n+1)(n^2+2n)}{3U^3}\right] + 2\left[\frac{n^2(n+1)^2}{U^3}(\beta U - 2)\right]$$
$$+ \frac{n(n+1)(n^2-1)}{3U^3} + \frac{n(n+1)(n^2+2n)}{3U^3}\right]$$
$$\left. + \left[\frac{2n^3(n+1)}{U^3} + \frac{n^2(n+1)^2}{U^3}(\beta U - 2)\right]\right\} \tag{82}$$

$$= \mathsf{t}_{jj'} \mathsf{t}_{j'j_1} \mathsf{t}_{j_1j'} \left\{ \frac{2n(n+1)(4n^2+4n+1)}{3U^3} \right.$$
$$\left. + 4 \frac{n^2(n+1)^2}{U^2} \beta \right\}. \quad (83)$$

Similarly, we find

$$\overline{\mathfrak{C}}_{jj_2jj'}^{(3)} = \mathsf{t}_{jj_2} \mathsf{t}_{j_2j} \mathsf{t}_{jj'} \left\{ \frac{2n(n+1)(4n^2+4n+1)}{3U^3} + 4 \frac{n^2(n+1)^2}{U^2} \beta \right\}. \quad (84)$$

Using these and Eq. (48), we get

$$C_{j'j}^{(3,1)} = - \left[\sum_{j_1} \mathsf{t}_{jj'} \mathsf{t}_{j'j_1} \mathsf{t}_{j_1j'} + \sum_{j_2} \mathsf{t}_{jj_2} \mathsf{t}_{j_2j} \mathsf{t}_{jj'} \right]$$
$$\times \left\{ \frac{2n(n+1)(26n^2+26n+5)}{3U^3} \right\}. \quad (85)$$

Next,

$$\overline{\mathfrak{C}}_{jj'jj'}^{(3)} = \mathsf{t}_{jj'} \mathsf{t}_{j'j} \mathsf{t}_{jj'} \left\{ 2 \left[2 \frac{n^2(n+1)^2}{U^3}(\beta U - 2) \right] \right.$$
$$\left. + 4 \left[\frac{n^2(n+1)^2}{U^3}(\beta U - 2) + \frac{4(n-1)n(n+1)(n+2)}{4U^3} \right] \right\} \quad (86)$$

$$= \mathsf{t}_{jj'} \mathsf{t}_{j'j} \mathsf{t}_{jj'} \left\{ 8 \frac{n^2(n+1)^2}{U^2} \beta - \frac{2n(n+1)(7n^2+7n+2)}{U^3} \right\}. \quad (87)$$

Hence, using Eq. (49), we obtain

$$C_{j'j}^{(3,2)} = [\mathsf{t}_{jj'} \mathsf{t}_{j'j} \mathsf{t}_{jj'}] \left\{ \frac{n(n+1)(23n^2+23n+2)}{3U^3} \right\}. \quad (88)$$

Note, again, the exact cancelation of the divergent temperature-dependent terms above. It is straightforward to verify that the Fourier transforms of the expressions for $C^{(m,0)}$ above up to third-order agree with those obtainable by expanding the RPA expression in powers of $\epsilon_{\mathbf{k}}$ (see below).

III. SCALING ANALYSIS

In the rest of this paper, we specialize to the case of nearest-neighbor hopping on a hypercubic lattice in d dimensions. Combining the different contributions for $C_{j'j}$ for such a lattice and Fourier transforming to momentum space, we arrive at the starting point for the scaling analysis, which is the strong-coupling expansion for the zero-temperature momentum distribution truncated to third order in the hopping and shown in Eq. (7). It is more convenient to re-express the results for different cases in terms of the dimensionless parameters $x = d\mathsf{t}/U$ and $\xi_{\mathbf{k}} = \epsilon_{\mathbf{k}}/2d\mathsf{t}$. If we further consider only the $n=1$ Mott insulator, we find

$$n_{\mathbf{k}} = 1 - 8\xi_{\mathbf{k}}x + \left[72\xi_{\mathbf{k}}^2 - \frac{36}{d} \right]x^2 - 32 \left[22\xi_{\mathbf{k}}^3 - \frac{19}{d} + \frac{2}{d^2} \right]x^3,$$
$$(89)$$

i.e.,

$$n_{\mathbf{k}} = 1 - 8\xi_{\mathbf{k}}x + 72\xi_{\mathbf{k}}^2 x^2 - 704\xi_{\mathbf{k}}^3 x^3, \quad (90)$$

in infinite dimensions where x remains finite as $d \to \infty$,

$$n_{\mathbf{k}} = 1 - 8\xi_{\mathbf{k}}x + 12[6\xi_{\mathbf{k}}^2 - 1]x^2 - 32 \left[22\xi_{\mathbf{k}}^2 - \frac{55}{9} \right]\xi_{\mathbf{k}}x^3$$
$$(91)$$

in three dimensions,

$$n_{\mathbf{k}} = 1 - 8\xi_{\mathbf{k}}x + 18[4\xi_{\mathbf{k}}^2 - 1]x^2 - 32[22\xi_{\mathbf{k}}^2 - 9]\xi_{\mathbf{k}}x^3 \quad (92)$$

in two dimensions, and

$$n_{\mathbf{k}} = 1 - 8\xi_{\mathbf{k}}x + 36[2\xi_{\mathbf{k}}^2 - 1]x^2 - 32[22\xi_{\mathbf{k}}^2 - 17]\xi_{\mathbf{k}}x^3 \quad (93)$$

in one dimension. Note that because integrals of odd powers of $\xi_{\mathbf{k}}$ over momentum vanish, we can use the fact that the integral of the square of $\xi_{\mathbf{k}}$ over $\mathbf{k}$ is equal to $1/2d$ to show that the integral of the strong-coupling expansion for $n_{\mathbf{k}}$ over $\mathbf{k}$ is always equal to 1, as it must be.

We show comparison of these truncated third-order strong-coupling expansions directly with exact numerical results and other analytic approximations below. It turns out that the truncated strong-coupling expansion does not work so well for the momentum distribution once the hopping is on the order of one-fourth of the critical hopping for the Mott-to-superfluid transition in two and three dimensions (and is even worse in one dimension). Hence, we use additional knowledge about the momentum distribution and how it scales near the critical point, along with the exact solution in large dimensions to create a phenomenological ansatz for the momentum distribution which produces analytical expressions useful for direct comparison with experiment. While there is always some amount of freedom allowed in phenomenological expressions, we strive to use the best available information that we have in order to produce the most accurate analytic expressions for the momentum distribution that we can, while still maintaining all of the required properties of the momentum distribution and its known limiting behavior.

We start our scaling analysis with a general discussion. The zero-momentum distribution function becomes critical at the critical value of the hopping for the Mott insulator–to–superfluid transition (called x_c). The critical behavior goes like $n_{\mathbf{k}=0} \to \xi^{(1-\eta)}$, where $\xi \propto 1/(x_c-x)^\nu$ is the correlation length of a $(d+1)$-dimensional XY model [2] and η and ν are critical exponents in the usual notation [30]. In two and higher dimensions, the correlation length diverges as a power law. The critical exponents for the two-dimensional Bose-Hubbard model, which correspond to the three-dimensional XY model, are $\eta = 0.04$ and $\nu = 0.67$, so $(1-\eta)\nu = \gamma_s = 0.64$. In three and higher dimensions for the Bose-Hubbard model, the critical exponents are mean-field-like, with $\eta = 0$ and $\nu = 0.5$, so $(1-\eta)\nu = \gamma_s = 0.5$. The one-dimensional case has Kosterlitz-Thouless behavior [31], where $\eta = 0.25$, and the divergence of the correlation length has a Kosterlitz-Thouless exponential form $\xi \propto \exp[W/\sqrt{x_c-x}]$, with x_c as the critical point for the Mott insulator–to–superfluid transition. By employing the information about the critical point into

our scaling analysis, we ensure that the results will be accurate near the critical point, which the truncated expansions to finite order can never achieve.

This critical scaling behavior does not provide enough information for us to determine an ansatz for the momentum distribution function over all momentum, because the distribution function is not critical for nonzero momentum. We use the exact solution in the infinite-dimensional limit, as given by the RPA solution, to guide us in how to proceed to develop an appropriate scaling ansatz. The RPA form for the momentum distribution function, as discussed above and re-expressed in terms of $\xi_{\mathbf{k}}$ and x, is given by [22]

$$n_{\mathbf{k}} = -\frac{1}{2} + \frac{n + \frac{1}{2} + \xi_{\mathbf{k}}x}{\sqrt{1 + 4(2n+1)\xi_{\mathbf{k}}x + 4\xi_{\mathbf{k}}^2 x^2}}, \qquad (94)$$

and this is the exact solution in infinite dimensions. A quick examination of the strong-coupling expansion for arbitrary dimensions shows that the $O(1)$ terms are the same for all dimensions, when expressed in terms of x and $\xi_{\mathbf{k}}$, and it is only the $1/d^n$ corrections that differ for the different dimensions. Hence, the power-series expansion of the RPA form must produce all of the $O(1)$ terms. In finite dimensions, only $1/d^n$ corrections are allowed. This motivates the following scaling ansatz for the momentum distribution function in two or higher dimensions (on a bipartite lattice):

$$n_{\mathbf{k}} = -\frac{1}{2}$$
$$+ \frac{n + \frac{1}{2} + \xi_{\mathbf{k}}x + \frac{c'}{d^2}x^2 + 2\frac{e'}{d^2}\xi_{\mathbf{k}}x^3}{\left[1 + 2\bar{a}\xi_{\mathbf{k}}x + 4\bar{b}\xi_{\mathbf{k}}^2 x^2 + \frac{\bar{c}}{d^2}x^2 + 8\bar{d}\xi_{\mathbf{k}}^3 x^3 + 2\frac{\bar{e}}{d^2}\xi_{\mathbf{k}}x^3\right]^{\gamma_s}}, \qquad (95)$$

with d as the spatial dimension. Note that in three dimensions, since $\gamma_s = 0.5$ which is the same power law as in infinite dimensions, we must have $\bar{d} = 0$. We will see this occur in the analysis below.

In order to determine the parameters in the scaling ansatz, we propose three requirements of the formula in Eq. (95): (i) the power-series expansion of the scaling ansatz, in powers of x, must reproduce the strong-coupling expansion through the given order (in our case through third order) as shown in Eq. (7); (ii) we choose the scaling form to have the exact critical point x_c, as determined by QMC, DMRG, or scaling results of a strong-coupling expansion for the phase diagram (in general the most accurate available data should be used, but if no sophisticated numerics is available, the scaling results from a third-order strong-coupling expansion for the phase diagram often are accurate to within a few percent for the critical point); and (iii) we require the integral of $n_{\mathbf{k}}$ over all momentum to give n, the density of the bosons in the Mott phase (sometimes this last constraint cannot be satisfied, in which case one takes the value closest to n). In two and higher dimensions, these three requirements will determine all of the parameters, which we now show. In one di-

mension, we use additional information to determine the Kosterlitz-Thouless constant W, which then allows us to determine the complete scaling form.

We begin with the infinite-dimensional case where the hopping scales like $1/d$ so that x is finite, but the coefficients $\bar{c}$, c', $\bar{e}$, and e' all vanish because they are $1/d^2$ corrections. Expanding the scaling ansatz in a power series in x and equating the coefficients of the powers of x with the strong-coupling expansion in Eq. (7) yields $\bar{a} = (2n+1)/\gamma_s = 2(2n+1)$, $\bar{b} = 1/2\gamma_s = 1$, and $\bar{d} = 0$, so we recover the RPA result in Eq. (94). Since the critical behavior occurs at the point where $1 + 4(2n+1)\xi_{\mathbf{k}}x_c + 4\xi_{\mathbf{k}}x_c^2 = 0$, and we evaluate for $\mathbf{k} = 0$, where $\xi_0 = -1$, we immediately find that $x_c = (n+1/2) - \sqrt{n(n+1)}$, which is the exact critical point [2,9] for all n. Hence, one can see that this approach automatically produces the right behavior for the large-dimensional limit.

Note that the curvature of the RPA momentum distribution, with respect to $\xi_{\mathbf{k}}$, is always one sign. In the truncated third-order strong-coupling expansion, the curvature of the momentum distribution function changes sign at $\xi_{\mathbf{k}} = 1$ when $x \approx 0.034$. This effect occurs for all finite dimensions as well. The scaled results, which are shown below, do not have a change in the sign of the curvature. We expect that this does not occur in any of the exact solutions of the Bose-Hubbard model.

Since the momentum distribution function depends on the correlation length at $\mathbf{k} = 0$, and so does the phase diagram, it is interesting to try a phenomenological exercise where we take the critical behavior determined via our scaling approach for the momentum distribution and relate it to a determination of the phase diagram. Since we have a power law of a polynomial, instead of the simplest scaling dependence, which would go like $\sqrt{x_c - x}$, such an approach is similar to summing an infinite number of terms in the expansion for the Mott-phase lobes in the phase diagram. As an example, we make the following scaling ansatz for the Mott lobes:

$$\left.\frac{\mu}{U}\right|_{\pm} = n + A(x) \pm B(x)[\text{scaling polynomial}]^{Z\nu}, \quad (96)$$

where the scaling polynomial is the polynomial used for the momentum distribution at $\mathbf{k} = 0$ [which is $1 - 4(2n+1)x + 4x^2$ for the infinite-dimensional case], and $A(x)$ and $B(x)$ are polynomials in x. Fitting the parameters to the third-order expansion for the Mott-phase lobes, we find for the infinite-dimensional case that

$$\left.\frac{\mu}{U}\right|_{\pm} = n - \frac{1}{2} - x \pm \frac{1}{2}\sqrt{1 - 4(2n+1)x + 4x^2}, \quad (97)$$

which is the exact solution [2,9].

In finite dimensions, we will consider only the $n = 1$ case, because good numerical data are available for the Mott-phase boundary in one, two, and three dimensions and we want to ensure that we produce the most accurate critical point x_c. We start with the three-dimensional case. Taking $n = 1$, we expand Eq. (95) in a power series in x, and compare with the strong-coupling expansion in Eq. (91). We find $\bar{a} = 6$, $\bar{b} = 1$,

$\bar{c} = 144 + 4c'/3$, $\bar{d} = 0$, and $\bar{e} = 224/3 + 58c'/9 + 4e'/3$. At this point, the constants c' and e' are not determined. We fix e', by requiring the momentum distribution at $\mathbf{k} = 0$ to diverge at the critical point $x_c = 0.102\,24$ as determined by QMC simulation [17]. This produces the equation

$$1 - 12x_c + \left(20 + \frac{4}{27}c'\right)x_c^2 - \left(\frac{448}{27} + \frac{116}{81}c' + \frac{8}{27}e'\right)x_c^3 = 0. \tag{98}$$

Setting $x_c = 0.102\,24$ and solving for e' yields

$$e' = -122.2743 + 0.057\,120\,5c'. \tag{99}$$

(Note that if we instead set the coefficients c' and e' to zero, then the critical point would lie at $x_c = 0.098\,05$, which is about a 4.3% error.) The coefficient c' is determined by requiring $\int d^3k n_{\mathbf{k}} = 1$; we find that c' ranges from 0 at $x = 0$ out to $c' = -1.86$ as $x \to x_c$. A simple polynomial fit to the behavior of $c'(x)$ is

$$c'(x) = 0.017\,166 - 0.719\,82x - 161.093x^2 - 109.614x^3. \tag{100}$$

We compare the strong-coupling perturbation theory to numerically exact results performed with world-line quantum Monte Carlo simulations of the Bose-Hubbard model that employ the directed-loop algorithm [32], in particular, its continuous-imaginary-time variant [33]. We have further improved the algorithm by omitting one-site vertices corresponding to the U term [34] and also two-body vertices corresponding to the hopping term [35]. The latter modification is useful in reducing the memory and was crucial in the present simulation of the largest system ($L = 64$). The accuracy of the method is tested by comparing with exact diagonalization for small systems, and verifies the critical exponents with known results for the $(d+1)$-dimensional XY model. To further test that the true equilibrium distribution is sampled on large systems, several independent runs with varying lattice sizes are carried out, showing no systematic deviation, thereby ensuring that our numerical results are "exact" except for statistical errors. This QMC approach has already been applied to the problem of determining how the momentum distribution changes when the system becomes superfluid [18].

We also compare the momentum distribution to RPA results. Since the RPA has a critical value of x that is smaller than the true critical value in finite dimensions, we plot the RPA results in Eq. (94) at a rescaled hopping value, corresponding to the same fractional amount of x_c. Namely, we choose $x_{RPA} = 0.085\,786\,4x/x_c(d)$. We call this the scaled RPA momentum distribution.

The scaled results of the strong-coupling perturbation theory fit the numerical QMC data quite well. We compare with data at $x = 0.0625$ and $x = 0.09$ in Figs. 7 and 8, respectively. The QMC data are for a $48 \times 48 \times 48$ lattice at a temperature $T = 0.1t$ ($T = 0.025t$ for $x = 0.09$). In all cases, we have carefully checked that the finite-size effects and the finite-temperature effects are much smaller than the symbol size in all of our results. Note how the QMC data follow the scaled curve much better than the strong-coupling curve, al-
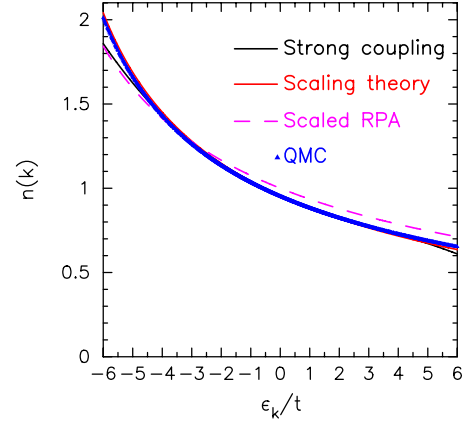

FIG. 7. (Color online) Momentum distribution function for the three-dimensional case with $x = 0.0625$ as a function of the band energy $\epsilon_{\mathbf{k}}$. Note how the QMC data agree better with the scaling-theory results than it does with the strong-coupling results or the scaled RPA, although deviations can be seen in the data. Both the scaling theory and the scaled RPA use the QMC critical point as an input.

though there are definitely differences between the two. The deviations between the QMC data and the scaling result are real and larger than the finite-size or finite-temperature effects. This simply reflects the fact that the scaling result is not an exact interpolation formula for the momentum distribution. As expected, the momentum distribution is peaked at zero momentum, and as one approaches the critical point at $x = 0.102\,24$, the peak becomes sharper. One can also see that the truncated third-order expansion is not too accurate. As we already mentioned above, the curvature for momenta near the zone boundary has the wrong sign even for quite small hopping. It also underestimates the size of the peak at zero momentum, and this gets worse as we approach the critical
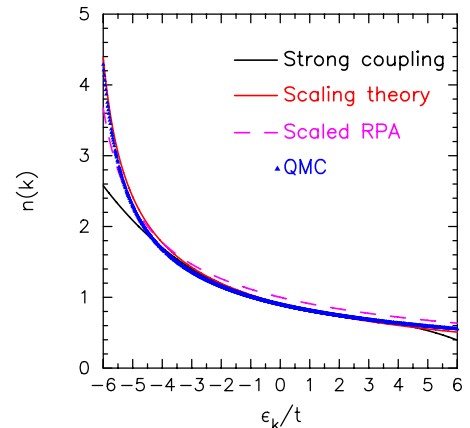

FIG. 8. (Color online) Momentum distribution function for the three-dimensional case with $x = 0.09$ as a function of the band energy $\epsilon_{\mathbf{k}}$. Once again, the QMC data agree better with the scaling theory than it does with the strong-coupling results or the scaled RPA, although deviations can still be seen in the data. Note that the scaled RPA works better than the truncated strong-coupling expansion. Both the scaling theory and the scaled RPA use the QMC critical point as an input.
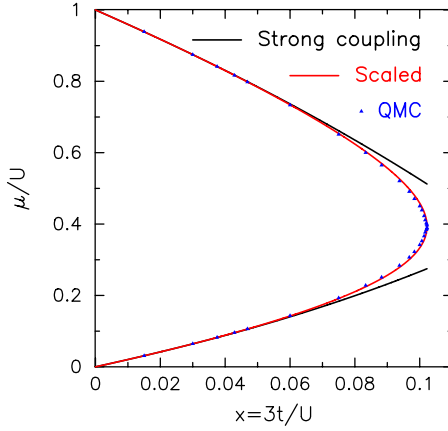
FIG. 9. (Color online) Phase diagram of the three-dimensional Bose-Hubbard model. Note how the truncated strong-coupling expansion does not agree so well with the QMC data [17], but the scaled results nearly fit the Mott-phase lobe perfectly.

point. Nevertheless, the strong-coupling expansion is quite accurate for small enough hopping. Moreover the fact that it agrees essentially exactly with both the scaled results and the QMC simulations provides an independent check that all of these different approaches are working to high precision.

We now try the phenomenological approach on the three-dimensional phase diagram. Here we have some uncertainty in how to proceed, because the scaling polynomial has freedom in our ability to vary the c' coefficient. We can either modify the scaling polynomial to represent the changes in c', or we can fix c' at a specific value and proceed from there. It turns out that we get better results if we fix $c'=0$ when calculating the phase diagram (especially for the two-dimensional case below). So we adopt that as our procedure (note we do not also set $e'=0$, because that would produce the wrong critical point for this phenomenological approach). The result for the Mott-phase lobes is

$$\left.\frac{\mu}{U}\right|_{\pm} = \frac{1}{2} - x - \frac{1}{2}x^2 + x^3 \pm \left[\frac{1}{2} - \frac{1}{2}x^2 - 8.815\,14x\right]$$
$$\times \sqrt{1 - 12x + 20x^2 + 16.673\,87x^3}. \quad (101)$$

These results are plotted versus the QMC calculations [17] in Fig. 9. One can see that while the truncated strong-coupling expansion [8,9] does not agree so well with the QMC data near the critical point, the agreement of the scaled curves is excellent.

Next, we move on to two dimensions. Recall that $\gamma_s = 0.64$ in this case. Going through the same procedure outlined above produces the following solution for the coefficients in the scaling polynomial: $\bar{a} = 3/\gamma_s = 4.6875$; $\bar{b} = -17/2\gamma_s + 9/2\gamma_s^2 = -2.294\,92$; $\bar{c} = 48/\gamma_s + 2c'/3\gamma_s = 75.0 + 1.041\,67c'$; $\bar{d} = 33/\gamma_s - 51/2\gamma_s^2 + 9/2\gamma_s^3 = 6.472\,78$; and $\bar{e} = -256/\gamma_s + 144/\gamma_s^2 - 2c'/9\gamma_s + 2c'/\gamma_s^2 + 2e'/3\gamma_s = -48.4375 + 4.535\,59c' + 1.041\,67e'$. Once again, c' and e' are as yet undetermined. We find e' by requiring the critical point at $\mathbf{k} = 0$ to occur at the QMC and strong-coupling critical point $x_c = 0.119\,48$ [16]. The critical point is found when
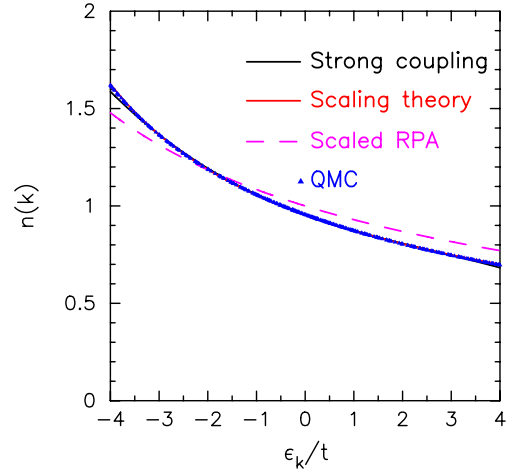

FIG. 10. (Color online) Momentum distribution function in two dimensions with $x = 0.05$. We plot the strong-coupling expansion against the scaling-theory results, the scaled RPA, and QMC simulations. Note how the QMC results agree much better with the scaled results and do not show the change in curvature near $\xi_\mathbf{k} = 1$. In addition, the scaled RPA does not work as well here as it did in three dimensions. Both the scaling theory and the scaled RPA use the QMC critical point as an input.

$$1 - 9.375x_c + (9.570\,32 + 0.260\,418c')x_c^2$$
$$+ (-27.563\,49 - 2.267\,80c' - 0.260\,418e')x_c^3 = 0. \quad (102)$$

(If we set $c' = e' = 0$, then the critical point would lie at $x_c = 0.115\,79$ which is a 3.2% error.) Substituting in $x_c = 0.119\,48$ then yields $e' = -68.7054 - 0.338\,706c'$. The parameter c' is then determined by requiring the integral of $n_\mathbf{k}$ over all momentum to equal one. We find that c' ranges from approximately -115 at $x = 0$ to $c' \approx -224$ at $x = 0.119$, but for values of x larger than about 0.1169, there is no value of c' that gives the total particle density to be exactly 1—the error is about 1.5% at $x = 0.119$ when we choose the best fit c'. A simple fit of $c'(x)$ is

$$c'(x) = -99 - 13.7(1 - 7.914x)^{-0.77}. \quad (103)$$

We compare our analytic expressions to QMC data in two dimensions on a 48×48 lattice with $T = 0.05$. In Fig. 10, we plot a case far from the critical point with $x = 0.05$. The scaling curve and the truncated strong-coupling expansion are both quite close to each other here, but one can see how the curvature has changed in the strong-coupling expansion but not in the data nor in the scaled curve. One also can see systematically that the QMC data agree better with the scaled curve than the strong-coupling expansion. Moving on to a point much closer to the critical point at $x = 0.1$, we show the same plots in Fig. 11 with the QMC data on a 48×48 lattice with $T = 0.006\,25$. Here, one can see a much more dramatic difference between the truncated strong-coupling results and the scaled results. While there definitely are some minor discrepancies with the QMC data and the scaled results, the agreement is, in general, outstanding. Note that we plot the momentum distribution versus $\epsilon_\mathbf{k}$ instead of $\mathbf{k}$, because in the
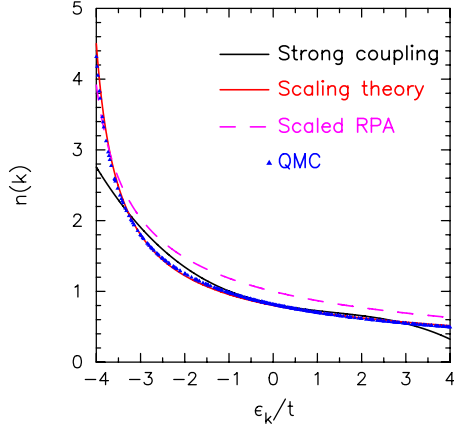
FIG. 11. (Color online) Momentum distribution function in two dimensions with $x=0.1$, which is close to the critical point. We plot the strong-coupling expansion against the scaling-theory results, the scaled RPA, and the QMC simulations. Note how the QMC results agree much better with the scaling-theory results. Both the scaling theory and the scaled RPA use the QMC critical point as an input.

strong-coupling expansion all momentum dependence is summarized in $\epsilon_{\mathbf{k}}$ through third order, so there is limited other momentum dependence. For the QMC data, we average the small number of degenerate energy values.

We finally try the phenomenological fit to the phase diagram by using the scaling polynomial in the power law and forcing the third-order strong-coupling expansion to agree with the phenomenological scaling ansatz. Once again, we set $c'=0$ when we do this, because the agreement is significantly worse with different c' values. Because c' assumes much larger values in two dimensions in order to get the right integrated weight in the momentum distribution, this is a significant assumption we are making, but as seen in the final results, the assumption seems reasonable because the agreement is quite good.

Following an identical procedure to what was done in the three-dimensional case (with c' set equal to zero), we find
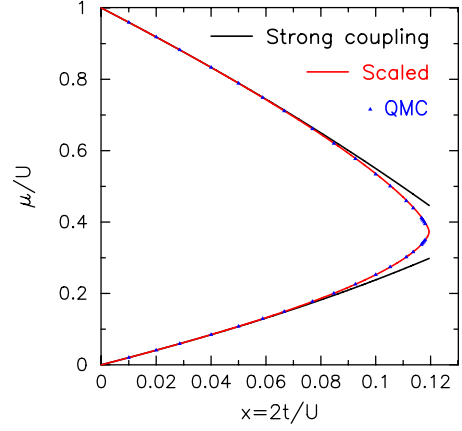
FIG. 12. (Color online) Phase diagram of the two-dimensional Bose-Hubbard model. Note how the truncated strong-coupling expansion [8,9] does not agree so well with the QMC data [16], but the scaled results nearly fit the Mott-phase lobe perfectly.

$$
\begin{aligned}
\frac{\mu}{U}\bigg|_{\pm} = {} & \frac{1}{2} - x - \frac{3}{4}x^2 + \frac{3}{2}x^3 \\
& \pm \left[\frac{1}{2} + 0.140\,63x - 0.214\,60x^2 - 3.870\,43x^3 \right] \\
& \times [1 - 9.375x + 9.5704x^2 - 9.6757x^3]^{0.67}. \quad (104)
\end{aligned}
$$

These results are plotted versus the QMC calculations [16] in Fig. 12. Once again note that while the truncated strong-coupling expansion does not agree so well with the QMC data near the critical point, the scaled curves lie essentially on top of the QMC data.

The one-dimensional case is different from higher dimensions because the scaling behavior is not power law, but instead is the Kosterlitz-Thouless form of the two-dimensional XY model. Hence, we modify our scaling ansatz to

$$
n_{\mathbf{k}} = -\frac{1}{2} + \left[n + \frac{1}{2} + \xi_{\mathbf{k}}x + c'x^2 + 2e'\xi_{\mathbf{k}}x^3 \right] \exp\left[-W' + \frac{W'}{\sqrt{1 + 2\bar{a}\xi_{\mathbf{k}}x + 4\bar{b}\xi_{\mathbf{k}}^2 x^2 + \bar{c}x^2 + 8\bar{d}\xi_{\mathbf{k}}^3 x^3 + 2\bar{e}\xi_{\mathbf{k}}x^3}} \right], \quad (105)
$$

which replaces the power-law divergence by the appropriate exponential divergence. Because the exponent $\eta = 0.25$ for the two-dimensional XY model, we have that $W' = 0.75W$, with W as the parameter in the Kosterlitz-Thouless fit to the one-dimensional Mott-phase diagram. Using the data of Elstner and Monien [14], we fit the gap function $\Delta(x)$ to the Kosterlitz-Thouless form

$$
[\ln \Delta(x)]^2 = \frac{A + Bx + Cx^2 + Dx^3 + Ex^4 + Fx^5 + Gx^6}{1 + Hx + Ix^2 + Jx^3 + Kx^4 + Lx^5 + Mx^6 + Nx^7},
$$

by using a Padé approximant for the pole that develops in the square of the logarithm of the gap function. Note that one

needs to do the Padé approximant for the square of the logarithm of the power series in order to obtain a robust fit [instead of doing a series or Padé approximation for $\Delta(x)$ first and then taking the square of the logarithm of the resulting series or Padé approximant]. The critical point is $x_c = 0.299\,81$ and the parameter W becomes $W = 1.7241$ or $W' = 1.2931$.

Now we solve for the coefficients in the scaling form just as we did in higher dimensions. First we ensure that the power-series expansion of the scaling form reproduces the strong-coupling expansion through the third order in x, then we ensure that the denominator of the square root in the
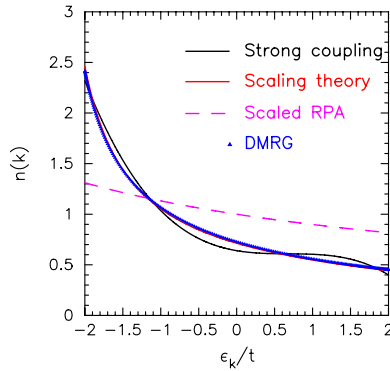
FIG. 13. (Color online) Momentum distribution function in one dimension with $x=0.1$, which is far from the critical point. We plot the strong-coupling expansion against the scaling-theory results, the scaled RPA, and the DMRG calculations. Note how the DMRG results agree much better with the scaling-theory results than the truncated expansion or the scaled RPA. Both the scaling theory and the scaled RPA use the DMRG critical point as an input.
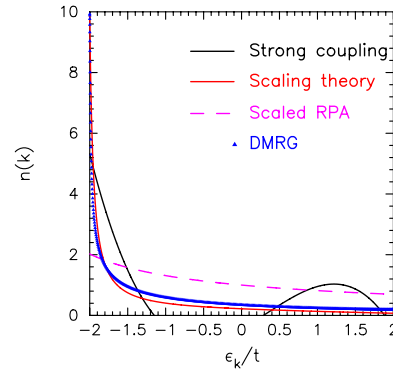

FIG. 14. (Color online) Momentum distribution function in one dimension with $x=0.2$, which is two-thirds of the way to the critical point. We plot the strong-coupling expansion against the scaling-theory results, the scaled RPA, and the DMRG calculations. Note how the DMRG results agree much better with the scaling-theory results than the truncated expansion or the scaled RPA, but one can see that the scaling approach is beginning to fail. Both the scaling theory and the scaled RPA use the DMRG critical point as an input.

exponential diverges at x_c. These two conditions yield $\bar{a}$ $=4.6400$, $\bar{b}=3.0006$, $\bar{c}=37.1201+1.0311c'$, $\bar{d}=9.4879$, $\bar{e}$ $=64.2632+6.8329c'$, and $e'=-9.4630-0.3190c'$. The coefficient c' is adjusted to guarantee that the integral of the momentum distribution over all momentum is equal to 1. We find that $c'\approx-7.92-15.16x$ in order to satisfy the sum rule.

We compare the scaled strong-coupling perturbation theory to the numerical calculations in one dimension from the DMRG approach [36] (provided to us by Kollath). Those calculations are essentially exact except for finite-size effects which become more important as we approach the critical point at $x=0.299\,81$. In Fig. 13, we compare the different approximations to the DMRG calculations. One can immediately see that although the truncated expansion has a non-monotonic dependence on $\epsilon_{\mathbf{k}}$, the scaled approach essentially agrees exactly with the DMRG calculations.

Next, we compare the different approximate results to the DMRG calculations for $x=0.2$ in Fig. 14. Here we see that while the scaled results still agree well with the DMRG results near $\mathbf{k}=0$, the agreement is not so good throughout the Brillouin zone, and it is clear that the approximation is becoming inadequate. When we compare results for large values of the hopping, such as $x=0.25$, the scaled results become negative over about half of the Brillouin zone, which is unphysical.

We do not go through the phenomenological exercise of comparing our results to the phase diagram in the one-dimensional case as we did previously for higher dimensions. This is primarily because we could see the approximate scaled results were breaking down around $x\approx0.2$, so it is unlikely that a phenomenological approach for the phase diagram would be accurate in this case. In general, the strong-coupling approach is more accurate in higher rather than lower dimensions.

IV. CONCLUSIONS

In this work, we have shown how one can generalize strong-coupling perturbation theory from an expansion for the many-body energy levels, or for different ground-state correlation functions, to a direct expansion for the many-body Green's function at finite temperature. Here, we focused on applying the expansion to the problem of determining the momentum distribution in the bulk for the Bose-Hubbard model within the Mott-insulating phase. By applying a scaling ansatz, which was motivated by recent work on the RPA, we are able to find accurate analytic expressions for the momentum distributions that hold nearly up to the critical point in two and three dimensions (the results for one dimension are not quite as good). In addition, we showed how one can apply the results for the momentum distribution function to create a phenomenological theory for the Mott-phase lobes. Comparing these results to QMC simulations showed excellent agreement in two and three dimensions.

The strong-coupling formalism as developed here can be used, as we have indicated, to obtain a strong-coupling expansion for the self-energy, and to include inhomogeneous features, such as a harmonic trap or disorder potential, and the effects of thermal excitations. It can also be readily adapted to nonequilibrium cases such as moving the origin of the trap or modulating the optical lattice depth for Bragg spectroscopy. The quantum Monte Carlo approach can be generalized to calculate dispersion relations, densities of states, and real-time dynamics. We intend to examine those problems in the future.

Note added. Recently, we became aware of a different approach [37] to determining high-order perturbation series terms for the phase diagram, which agree well with the analytical forms for the phase diagrams that we plotted in two and three dimensions.

APPENDIX A: IMAGINARY TIME INTEGRALS NEEDED FOR THE STRONG-COUPLING EXPANSION

Consider the imaginary time-ordered integral

$$
I_m(\beta;\mathcal{E}_{\alpha_0},\mathcal{E}_{\alpha_m},\dots,\mathcal{E}_{\alpha_1}) \equiv \frac{e^{-\beta\mathcal{E}_{\alpha_0}}}{3}\int_0^\beta d\tau_m \int_0^{\tau_m} d\tau_{m-1}\cdots\int_0^{\tau_2}
$$
$$
\times d\tau_1 e^{[\tau_m(\mathcal{E}_{\alpha_0}-\mathcal{E}_{\alpha_m})+\tau_{m-1}(\mathcal{E}_{\alpha_m}-\mathcal{E}_{\alpha_{m-1}})+\cdots+\tau_2(\mathcal{E}_{\alpha_3}-\mathcal{E}_{\alpha_2})+\tau_1(\mathcal{E}_{\alpha_2}-\mathcal{E}_{\alpha_1})]}.
$$

(A1)

It is easy to see that the sequence of functions I_m satisfy the recursion relation:

$$
I_m(\tau;\mathcal{E}_{\alpha_0},\mathcal{E}_{\alpha_m},\dots,\mathcal{E}_{\alpha_1})
$$
$$
= \int_0^\tau d\tau' e^{-(\tau-\tau')\mathcal{E}_{\alpha_0}} I_{m-1}(\tau';\mathcal{E}_{\alpha_m},\mathcal{E}_{\alpha_{m-1}}\dots,\mathcal{E}_{\alpha_1}).
$$

(A2)

Taking the Laplace transform of both sides, it is straightforward to see that

$$
\mathcal{L}[I_m(\tau;\mathcal{E}_{\alpha_0},\mathcal{E}_{\alpha_m},\dots,\mathcal{E}_{\alpha_1});s]
$$
$$
\equiv \int_0^\infty d\tau e^{-s\tau} I_m(\tau;\mathcal{E}_{\alpha_0},\mathcal{E}_{\alpha_m},\dots,\mathcal{E}_{\alpha_1})
$$
$$
= \int_0^\infty d\tau \int_0^\tau d\tau' e^{-s\tau} e^{-(\tau-\tau')\mathcal{E}_{\alpha_0}} I_{m-1}(\tau';\mathcal{E}_{\alpha_m},\mathcal{E}_{\alpha_{m-1}},\dots,\mathcal{E}_{\alpha_1})
$$

$$
= \int_0^\infty d\tau' \int_{\tau'}^\infty d\tau e^{-(s+\mathcal{E}_{\alpha_0})\tau} e^{\tau'\mathcal{E}_{\alpha_0}} I_{m-1}(\tau';\mathcal{E}_{\alpha_m},\mathcal{E}_{\alpha_{m-1}},\dots,\mathcal{E}_{\alpha_1})
$$
$$
= \int_0^\infty d\tau' \frac{e^{-s\tau'}}{s+\mathcal{E}_{\alpha_0}} I_{m-1}(\tau';\mathcal{E}_{\alpha_m},\mathcal{E}_{\alpha_{m-1}},\dots,\mathcal{E}_{\alpha_1})
$$
$$
= \frac{1}{s+\mathcal{E}_{\alpha_0}}\mathcal{L}[I_{m-1}(\tau;\mathcal{E}_{\alpha_m},\mathcal{E}_{\alpha_{m-1}},\dots,\mathcal{E}_{\alpha_1});s]. \quad (A3)
$$

Iterating this and noting that $I_0(\tau;\mathcal{E}_{\alpha_1})=e^{-\tau\mathcal{E}_{\alpha_1}}/3$, which implies that $\mathcal{L}[I_0(\tau;\mathcal{E}_{\alpha_1});s]=[3(s+\mathcal{E}_{\alpha_1})]^{-1}$, we find

$$
\mathcal{L}[I_m(\tau;\mathcal{E}_{\alpha_0},\mathcal{E}_{\alpha_m},\dots,\mathcal{E}_{\alpha_1});s]=\frac{1}{3}\prod_{\ell=0,m}\frac{1}{(s+\mathcal{E}_{\alpha_\ell})}. \quad (A4)
$$

Taking the inverse Laplace transform yields

$$
I_m(\tau;\mathcal{E}_{\alpha_0},\mathcal{E}_{\alpha_m},\dots,\mathcal{E}_{\alpha_1})=\int_{\gamma-i\infty}^{\gamma+i\infty}\frac{ds}{2\pi i}\frac{e^{\tau s}}{3}\prod_{\ell=0,m}\frac{1}{(s+\mathcal{E}_{\alpha_\ell})},
$$

(A5)

with $\gamma>\max(\mathcal{E}_{\alpha_0},\mathcal{E}_{\alpha_m},\dots,\mathcal{E}_{\alpha_1})$, so that all the singularities of the integrand lie to the left of the integration contour in the complex s plane. The integral is straightforwardly evaluated using the contour integration techniques. When all the energies $\mathcal{E}_{\alpha_0},\mathcal{E}_{\alpha_m},\dots,\mathcal{E}_{\alpha_1}$ are distinct, we get one contribution from each of the $m+1$ simple poles of the integrand in Eq. (A5), leading to Eq. (51). If one and only one pair of energies are equal, say, $\mathcal{E}_{\alpha_r}=\mathcal{E}_{\alpha_p}$, then the integrand of Eq. (A5) has $m-1$ simple poles and one double pole, and we get Eq. (52). One can similarly extend the results to other cases, corresponding to two double poles, or one triple pole, etc.

APPENDIX B: FINAL RESULTS FOR THE THIRD-ORDER EXPANSION TERMS

Explicit forms for the third-order coefficients in the strong-coupling expansion are presented here (for brevity only in the second form, as discussed in Sec. II):

$$
\mathfrak{C}^{(3)}_{jj_2j_1j'} = \mathfrak{t}_{jj_2}\mathfrak{t}_{j_2j_1}\mathfrak{t}_{j_1j'}\sum_{n,n_1,n_2,n'}\rho_{j,n}\rho_{j_1,n_1}\rho_{j_2,n_2}\rho_{j',n'}\left\{\left[\frac{n(n_2+1)(n_1+1)(n'+1)}{(\epsilon^-_{j,n}+\epsilon^+_{j_2,n_2})(\epsilon^-_{j,n}+\epsilon^+_{j_1,n_1})(\epsilon^-_{j,n}+\epsilon^+_{j',n'_j})}\right.\right.
$$
$$
+\frac{(n+1)(n_2+1)n_1(n'+1)}{(\epsilon^+_{j,n}+\epsilon^-_{j_1,n_1})(\epsilon^-_{j_1,n_1}+\epsilon^+_{j_2,n_2})(\epsilon^-_{j_1,n_1}+\epsilon^+_{j',n'})}+\frac{(n+1)(n_2+1)(n_1+1)n'}{(\epsilon^+_{j,n}+\epsilon^-_{j',n'})(\epsilon^+_{j_2,n_2}+\epsilon^-_{j',n'})(\epsilon^+_{j_1,n_1}+\epsilon^-_{j',n'})}
$$
$$
\left.+\frac{(n+1)n_2(n_1+1)(n'+1)}{(\epsilon^+_{j,n}+\epsilon^-_{j_2,n_2})(\epsilon^+_{j_1,n_1}+\epsilon^-_{j_2,n_2})(\epsilon^-_{j_2,n_2}+\epsilon^+_{j',n'})}\right]+\left[\frac{nn_2(n_1+1)(n'+1)}{(\epsilon^-_{j,n}+\epsilon^+_{j',n'})(\epsilon^-_{j,n}+\epsilon^+_{j_1,n_1})(\epsilon^-_{j_2,n_2}+\epsilon^+_{j_1,n_1})}\right.
$$

$$+ \frac{(n+1)n_2 n_1 (n'+1)}{(\epsilon^+_{j,n} + \epsilon^-_{j_2,n_2})(\epsilon^+_{j,n} + \epsilon^-_{j_1,n_1})(\epsilon^-_{j_1,n_1} + \epsilon^+_{j',n'})} + \frac{(n+1)n_2(n_1+1)n'}{(\epsilon^+_{j,n} + \epsilon^-_{j_2,n_2} + \epsilon^+_{j_1,n_1} + \epsilon^-_{j',n'})(\epsilon^+_{j_1,n_1} + \epsilon^-_{j',n'})(\epsilon^+_{j,n} + \epsilon^-_{j',n'})}$$

$$+ \frac{n(n_2+1)n_1(n'+1)}{(\epsilon^-_{j,n} + \epsilon^+_{j_2,n_2} + \epsilon^-_{j_1,n_1} + \epsilon^+_{j',n'})(\epsilon^-_{j,n} + \epsilon^+_{j_2,n_2})(\epsilon^+_{j_2,n_2} + \epsilon^-_{j_1,n_1})} \Bigg] + \Bigg[\frac{nn_2(n_1+1)(n'+1)}{(\epsilon^-_{j,n} + \epsilon^+_{j',n'})(\epsilon^-_{j_2,n_2} + \epsilon^+_{j_1,n_1})(\epsilon^-_{j_2,n_2} + \epsilon^+_{j',n'})}$$

$$+ \frac{n(n_2+1)(n_1+1)n'}{(\epsilon^-_{j,n} + \epsilon^+_{j_2,n_2})(\epsilon^-_{j_2,n_2} + \epsilon^+_{j',n'})(\epsilon^+_{j_1,n_1} + \epsilon^-_{j',n'})} + \frac{(n+1)n_2(n_1+1)n'}{(\epsilon^+_{j,n} + \epsilon^-_{j_2,n_2} + \epsilon^+_{j_1,n_1} + \epsilon^-_{j',n'})(\epsilon^+_{j,n} + \epsilon^-_{j_2,n_2})(\epsilon^+_{j,n} + \epsilon^-_{j',n'})}$$

$$+ \frac{n(n_2+1)n_1(n'+1)}{(\epsilon^-_{j,n} + \epsilon^+_{j_2,n_2} + \epsilon^-_{j_1,n_1} + \epsilon^+_{j',n'})(\epsilon^+_{j_2,n_2} + \epsilon^-_{j_1,n_1})(\epsilon^-_{j_1,n_1} + \epsilon^+_{j',n'})} \Bigg]$$

$$+ \Bigg[\frac{n(n_2+1)n_1(n'+1)}{(\epsilon^-_{j,n} + \epsilon^+_{j_2,n_2} + \epsilon^-_{j_1,n_1} + \epsilon^+_{j',n'})(\epsilon^-_{j,n} + \epsilon^+_{j_2,n_2})(\epsilon^-_{j,n} + \epsilon^+_{j',n'})}$$

$$+ \frac{(n+1)n_2(n_1+1)n'}{(\epsilon^+_{j,n} + \epsilon^-_{j_2,n_2} + \epsilon^+_{j_1,n_1} + \epsilon^-_{j',n'})(\epsilon^-_{j_2,n_2} + \epsilon^+_{j_1,n_1})(\epsilon^+_{j_1,n_1} + \epsilon^-_{j',n'})} + \frac{(n+1)n_2 n_1(n'+1)}{(\epsilon^+_{j,n} + \epsilon^-_{j_2,n_2})(\epsilon^-_{j_2,n_2} + \epsilon^+_{j',n'})(\epsilon^-_{j_1,n_1} + \epsilon^+_{j',n'})}$$

$$+ \frac{(n+1)(n_2+1)n_1 n'}{(\epsilon^+_{j_2,n_2} + \epsilon^-_{j_1,n_1})(\epsilon^+_{j_2,n_2} + \epsilon^-_{j',n'})(\epsilon^+_{j,n} + \epsilon^-_{j',n'})} \Bigg] + \Bigg[\frac{n(n_2+1)n_1(n'+1)}{(\epsilon^-_{j,n} + \epsilon^+_{j_2,n_2} + \epsilon^-_{j_1,n_1} + \epsilon^+_{j',n'})(\epsilon^-_{j,n} + \epsilon^+_{j',n'})(\epsilon^-_{j_1,n_1} + \epsilon^+_{j',n'})}$$

$$+ \frac{(n+1)n_2(n_1+1)n'}{(\epsilon^+_{j,n} + \epsilon^-_{j_2,n_2} + \epsilon^+_{j_1,n_1} + \epsilon^-_{j',n'})(\epsilon^+_{j,n} + \epsilon^-_{j_2,n_2})(\epsilon^-_{j_2,n_2} + \epsilon^+_{j_1,n_1})} + \frac{(n+1)(n_2+1)n_1 n'}{(\epsilon^+_{j,n} + \epsilon^-_{j_1,n_1})(\epsilon^+_{j_2,n_2} + \epsilon^-_{j_1,n_1})(\epsilon^+_{j,n} + \epsilon^-_{j',n'})}$$

$$+ \frac{n(n_2+1)(n_1+1)n'}{(\epsilon^-_{j,n} + \epsilon^+_{j_2,n_2})(\epsilon^-_{j,n} + \epsilon^+_{j_1,n_1})(\epsilon^+_{j_1,n_1} + \epsilon^-_{j',n'})} \Bigg] + \Bigg[\frac{nn_2 n_1(n'+1)}{(\epsilon^-_{j,n} + \epsilon^+_{j',n'})(\epsilon^-_{j_2,n_2} + \epsilon^+_{j',n'})(\epsilon^-_{j_1,n_1} + \epsilon^+_{j',n'})}$$

$$+ \frac{n(n_2+1)n_1 n'}{(\epsilon^-_{j,n} + \epsilon^+_{j_2,n_2})(\epsilon^+_{j_2,n_2} + \epsilon^-_{j_1,n_1})(\epsilon^+_{j_2,n_2} + \epsilon^-_{j',n'})} + \frac{(n+1)n_2 n_1 n'}{(\epsilon^+_{j,n} + \epsilon^-_{j_2,n_2})(\epsilon^+_{j,n} + \epsilon^-_{j_1,n_1})(\epsilon^+_{j,n} + \epsilon^-_{j',n'})}$$

$$+ \frac{nn_2(n_1+1)n'}{(\epsilon^-_{j,n} + \epsilon^+_{j_1,n_1})(\epsilon^-_{j_2,n_2} + \epsilon^+_{j_1,n_1})(\epsilon^+_{j_1,n_1} + \epsilon^-_{j',n'})} \Bigg], \tag{B1}$$

$$\overline{\mathfrak{C}}^{(3)}_{jj'j_1 j'} = t_{jj'} t_{j'j_1} t_{j_1 j'} \sum_{n,n_1,n'} \rho_{j,n} \rho_{j_1,n_1} \rho_{j',n'} \Bigg\{ \Bigg[\frac{n(n'+1)(n_1+1)(n'+1)}{(\epsilon^-_{j,n} + \epsilon^+_{j',n'_j})(\epsilon^-_{j,n} + \epsilon^+_{j_1,n_1})(\epsilon^-_{j,n} + \epsilon^+_{j',n'_j})} + \frac{(n+1)(n'+1)n_1(n'+1)}{(\epsilon^-_{j_1,n_1} + \epsilon^+_{j',n'})(\epsilon^+_{j,n} + \epsilon^-_{j_1,n_1})(\epsilon^-_{j_1,n_1} + \epsilon^+_{j',n'})}$$

$$+ \frac{(n+1)n'(n_1+1)n'}{(\epsilon^+_{j,n} + \epsilon^-_{j',n'})(\epsilon^+_{j_1,n_1} + \epsilon^-_{j',n'})} \left(\beta - \frac{1}{(\epsilon^+_{j,n} + \epsilon^-_{j',n'})} - \frac{1}{(\epsilon^+_{j_1,n_1} + \epsilon^-_{j',n'})} \right) \Bigg] + \Bigg[\frac{nn'(n_1+1)(n'+1)}{(\epsilon^-_{j,n} + \epsilon^+_{j_1,n_1})(\epsilon^+_{j_1,n_1} + \epsilon^-_{j',n'})(\epsilon^-_{j,n} + \epsilon^+_{j',n'})}$$

$$+ \frac{(n+1)n'n_1(n'+1)}{(\epsilon^+_{j,n} + \epsilon^-_{j_1,n_1})(\epsilon^+_{j,n} + \epsilon^-_{j',n'})(\epsilon^-_{j_1,n_1} + \epsilon^+_{j',n'})} + \frac{(n+1)(n'-1)(n_1+1)n'}{(\epsilon^+_{j,n} + \epsilon^-_{j',n'-1} + \epsilon^+_{j_1,n_1} + \epsilon^-_{j',n'})(\epsilon^+_{j_1,n_1} + \epsilon^-_{j',n'})(\epsilon^+_{j,n} + \epsilon^-_{j',n'})}$$

$$+ \frac{n(n'+2)n_1(n'+1)}{(\epsilon^-_{j,n} + \epsilon^+_{j',n'+1} + \epsilon^-_{j_1,n_1} + \epsilon^+_{j',n'})(\epsilon^-_{j,n} + \epsilon^+_{j',n'})(\epsilon^-_{j_1,n_1} + \epsilon^+_{j',n'})} \Bigg]$$

$$+ \Bigg[\frac{nn'(n_1+1)(n'+1)}{(\epsilon^-_{j,n} + \epsilon^+_{j',n'})(\epsilon^+_{j_1,n_1} + \epsilon^-_{j',n'})} \left(\beta - \frac{1}{(\epsilon^-_{j,n} + \epsilon^+_{j',n'})} - \frac{1}{(\epsilon^+_{j_1,n_1} + \epsilon^-_{j',n'})} \right)$$

$$+ \frac{(n+1)(n'-1)(n_1+1)n'}{(\epsilon^+_{j,n} + \epsilon^-_{j',n'-1} + \epsilon^+_{j_1,n_1} + \epsilon^-_{j',n'})(\epsilon^+_{j,n} + \epsilon^-_{j',n'})(\epsilon^+_{j,n} + \epsilon^-_{j',n'})}$$

$$+ \frac{n(n'+1)n_1(n'+2)}{(\epsilon^-_{j,n} + \epsilon^+_{j',n'} + \epsilon^-_{j_1,n_1} + \epsilon^+_{j',n'+1})(\epsilon^+_{j',n'} + \epsilon^-_{j_1,n_1})(\epsilon^-_{j_1,n_1} + \epsilon^+_{j',n'})} \Bigg]$$

$$+\left[\frac{n(n'+2)n_1(n'+1)}{(\epsilon^-_{j,n}+\epsilon^+_{j',n'+1}+\epsilon^-_{j_1,n_1}+\epsilon^+_{j',n'})(\epsilon^-_{j,n}+\epsilon^+_{j',n'})(\epsilon^-_{j,n}+\epsilon^+_{j',n'})}\right.$$

$$+\frac{(n+1)(n'-1)(n_1+1)n'}{(\epsilon^+_{j,n}+\epsilon^-_{j',n'-1}+\epsilon^+_{j_1,n_1}+\epsilon^-_{j',n'})(\epsilon^-_{j',n'}+\epsilon^+_{j_1,n_1})(\epsilon^+_{j_1,n_1}+\epsilon^-_{j',n'})}$$

$$+\left.\frac{(n+1)n'n_1(n'+1)}{(\epsilon^+_{j,n}+\epsilon^-_{j',n'})(\epsilon^-_{j_1,n_1}+\epsilon^+_{j',n'})}\left(\beta-\frac{1}{(\epsilon^+_{j,n}+\epsilon^-_{j',n'})}-\frac{1}{(\epsilon^-_{j_1,n_1}+\epsilon^+_{j',n'})}\right)\right]$$

$$+\left[\frac{n(n'+2)n_1(n'+1)}{(\epsilon^-_{j,n}+\epsilon^+_{j',n'+1}+\epsilon^-_{j_1,n_1}+\epsilon^+_{j',n'})(\epsilon^-_{j,n}+\epsilon^+_{j',n'})(\epsilon^-_{j_1,n_1}+\epsilon^+_{j',n'})}\right.$$

$$+\frac{(n+1)n'(n_1+1)(n'-1)}{(\epsilon^+_{j,n}+\epsilon^-_{j',n'}+\epsilon^+_{j_1,n_1}+\epsilon^-_{j',n'-1})(\epsilon^+_{j,n}+\epsilon^-_{j',n'})(\epsilon^-_{j',n'}+\epsilon^+_{j_1,n_1})}+\frac{(n+1)(n'+1)n_1n'}{(\epsilon^+_{j,n}+\epsilon^-_{j_1,n_1})(\epsilon^+_{j',n'}+\epsilon^-_{j_1,n_1})(\epsilon^+_{j,n}+\epsilon^-_{j',n'})}$$

$$+\left.\frac{n(n'+1)(n_1+1)n'}{(\epsilon^-_{j,n}+\epsilon^+_{j',n'})(\epsilon^-_{j,n}+\epsilon^+_{j_1,n_1})(\epsilon^+_{j_1,n_1}+\epsilon^-_{j',n'})}\right]+\left[\frac{n(n'+1)n_1(n'+1)}{(\epsilon^-_{j,n}+\epsilon^+_{j',n'})(\epsilon^-_{j_1,n_1}+\epsilon^+_{j',n'})}\left(\beta-\frac{1}{(\epsilon^-_{j,n}+\epsilon^+_{j',n'})}-\frac{1}{(\epsilon^-_{j_1,n_1}+\epsilon^+_{j',n'})}\right)\right.$$

$$+\frac{(n+1)n'n_1n'}{(\epsilon^+_{j,n}+\epsilon^-_{j',n'})(\epsilon^+_{j,n}+\epsilon^-_{j_1,n_1})(\epsilon^+_{j,n}+\epsilon^-_{j',n'})}+\left.\frac{nn'(n_1+1)n'}{(\epsilon^-_{j,n}+\epsilon^+_{j_1,n_1})(\epsilon^-_{j',n'}+\epsilon^+_{j_1,n_1})(\epsilon^+_{j_1,n_1}+\epsilon^-_{j',n'})}\right].\tag{B2}$$

Similarly, we get

$$\overline{\mathfrak{C}}^{(3)}_{jj_2jj'}=\mathfrak{t}_{jj_2}\mathfrak{t}_{j_2j}\mathfrak{t}_{jj'}\sum_{n,n_2,n'}\rho_{j,n}\rho_{j_2,n_2}\rho_{j',n'}\left\{\left[\frac{n(n_2+1)n(n'+1)}{(\epsilon^-_{j,n}+\epsilon^+_{j_2,n_2})(\epsilon^-_{j,n}+\epsilon^+_{j',n'_j})}\left(\beta-\frac{1}{(\epsilon^-_{j,n}+\epsilon^+_{j_2,n_2})}-\frac{1}{(\epsilon^-_{j,n}+\epsilon^+_{j',n'_j})}\right)\right.\right.$$

$$+\left.\frac{(n+1)(n_2+1)(n+1)n'}{(\epsilon^+_{j,n}+\epsilon^-_{j',n'})(\epsilon^+_{j_2,n_2}+\epsilon^-_{j',n'})(\epsilon^+_{j,n}+\epsilon^-_{j',n'})}+\frac{(n+1)n_2(n+1)(n'+1)}{(\epsilon^+_{j,n}+\epsilon^-_{j_2,n_2})(\epsilon^+_{j,n}+\epsilon^-_{j_2,n_2})(\epsilon^-_{j_2,n_2}+\epsilon^+_{j',n'})}\right]$$

$$+\left[\frac{nn_2(n+1)(n'+1)}{(\epsilon^-_{j,n}+\epsilon^+_{j',n'})(\epsilon^-_{j_2,n_2}+\epsilon^+_{j,n})}\left(\beta-\frac{1}{(\epsilon^-_{j,n}+\epsilon^+_{j',n'})}-\frac{1}{(\epsilon^-_{j_2,n_2}+\epsilon^+_{j,n})}\right)\right.$$

$$+\left.\frac{(n+1)n_2(n+2)n'}{(\epsilon^+_{j,n}+\epsilon^-_{j_2,n_2}+\epsilon^+_{j,n+1}+\epsilon^-_{j',n'})(\epsilon^+_{j,n}+\epsilon^-_{j',n'})(\epsilon^+_{j,n}+\epsilon^-_{j',n'})}+\frac{n(n_2+1)(n-1)(n'+1)}{(\epsilon^-_{j,n}+\epsilon^+_{j_2,n_2}+\epsilon^-_{j,n-1}+\epsilon^+_{j',n'})(\epsilon^-_{j,n}+\epsilon^+_{j_2,n_2})(\epsilon^-_{j_2,n_2}+\epsilon^+_{j,n})}\right]$$

$$+\left[\frac{nn_2(n+1)(n'+1)}{(\epsilon^-_{j,n}+\epsilon^+_{j',n'})(\epsilon^-_{j_2,n_2}+\epsilon^+_{j,n})(\epsilon^-_{j_2,n_2}+\epsilon^+_{j',n'})}+\frac{n(n_2+1)(n+1)n'}{(\epsilon^-_{j,n}+\epsilon^+_{j_2,n_2})(\epsilon^+_{j_2,n_2}+\epsilon^-_{j',n'})(\epsilon^+_{j,n}+\epsilon^-_{j',n'})}\right.$$

$$+\frac{(n+1)n_2(n+2)n'}{(\epsilon^+_{j,n}+\epsilon^-_{j_2,n_2}+\epsilon^+_{j,n+1}+\epsilon^-_{j',n'})(\epsilon^+_{j,n}+\epsilon^-_{j_2,n_2})(\epsilon^+_{j,n}+\epsilon^-_{j',n'})}$$

$$+\left.\frac{n(n_2+1)(n-1)(n'+1)}{(\epsilon^-_{j,n}+\epsilon^+_{j_2,n_2}+\epsilon^-_{j,n-1}+\epsilon^+_{j',n'})(\epsilon^+_{j_2,n_2}+\epsilon^-_{j,n})(\epsilon^-_{j,n}+\epsilon^+_{j',n'})}\right]$$

$$+\left[\frac{n(n_2+1)(n-1)(n'+1)}{(\epsilon^-_{j,n}+\epsilon^+_{j_2,n_2}+\epsilon^-_{j,n-1}+\epsilon^+_{j',n'})(\epsilon^-_{j,n}+\epsilon^+_{j_2,n_2})(\epsilon^-_{j,n}+\epsilon^+_{j',n'})}\right.$$

$$+\frac{(n+1)n_2(n+2)n'}{(\epsilon^+_{j,n}+\epsilon^-_{j_2,n_2}+\epsilon^+_{j,n+1}+\epsilon^-_{j',n'})(\epsilon^-_{j_2,n_2}+\epsilon^+_{j,n})(\epsilon^+_{j,n}+\epsilon^-_{j',n'})}$$

$$+\left.\frac{(n+1)(n_2+1)nn'}{(\epsilon^+_{j_2,n_2}+\epsilon^-_{j,n})(\epsilon^+_{j_2,n_2}+\epsilon^-_{j',n'})(\epsilon^+_{j,n}+\epsilon^-_{j',n'})}+\frac{(n+1)n_2n(n'+1)}{(\epsilon^+_{j,n}+\epsilon^-_{j_2,n_2})(\epsilon^-_{j_2,n_2}+\epsilon^+_{j',n'})(\epsilon^-_{j,n}+\epsilon^+_{j',n'})}\right]$$

$$+\left[\frac{n(n_2+1)(n-1)(n'+1)}{(\epsilon^-_{j,n}+\epsilon^+_{j_2,n_2}+\epsilon^-_{j,n-1}+\epsilon^+_{j',n'})(\epsilon^-_{j,n}+\epsilon^+_{j',n'})(\epsilon^-_{j,n}+\epsilon^+_{j',n'})}\right.$$

$$
+ \frac{(n+1)n_2(n+2)n'}{(\epsilon^+_{j,n} + \epsilon^-_{j_2,n_2} + \epsilon^+_{j,n+1} + \epsilon^-_{j',n'})(\epsilon^+_{j,n} + \epsilon^-_{j_2,n_2})(\epsilon^-_{j_2,n_2} + \epsilon^+_{j,n})}
$$

$$
+ \frac{(n+1)(n_2+1)nn'}{(\epsilon^+_{j_2,n_2} + \epsilon^-_{j,n})(\epsilon^+_{j,n} + \epsilon^-_{j',n'})}\left(\beta - \frac{1}{(\epsilon^+_{j_2,n_2} + \epsilon^-_{j,n})} - \frac{1}{(\epsilon^+_{j,n} + \epsilon^-_{j',n'})}\right)\Bigg] + \Bigg[\frac{nn_2n(n'+1)}{(\epsilon^-_{j,n} + \epsilon^+_{j',n'})(\epsilon^-_{j_2,n_2} + \epsilon^+_{j',n'})(\epsilon^-_{j,n} + \epsilon^+_{j',n'})}
$$

$$
+ \frac{n(n_2+1)nn'}{(\epsilon^-_{j,n} + \epsilon^+_{j_2,n_2})(\epsilon^+_{j_2,n_2} + \epsilon^-_{j,n})(\epsilon^+_{j_2,n_2} + \epsilon^-_{j',n'})} + \frac{(n+1)n_2(n+1)n'}{(\epsilon^+_{j,n} + \epsilon^-_{j_2,n_2})(\epsilon^+_{j,n} + \epsilon^-_{j',n'})}\left(\beta - \frac{1}{(\epsilon^+_{j,n} + \epsilon^-_{j_2,n_2})} - \frac{1}{(\epsilon^+_{j,n} + \epsilon^-_{j',n'})}\right)\Bigg]\Bigg],
$$

$$(B3)$$

and

$$
\overline{\mathfrak{C}}^{(3)}_{jj'jj'} = \mathfrak{t}_{jj'}\mathfrak{t}_{j'j}\mathfrak{t}_{jj'}\sum_{n,n'} \rho_{j,n}\rho_{j',n'}\Bigg\{\Bigg[\frac{n(n'+1)n(n'+1)}{(\epsilon^-_{j,n} + \epsilon^+_{j',n'_j})(\epsilon^-_{j,n} + \epsilon^+_{j',n'_j})}\left(\beta - \frac{2}{(\epsilon^-_{j,n} + \epsilon^+_{j',n'_j})}\right)
$$

$$
+ \frac{(n+1)n'(n+1)n'}{(\epsilon^+_{j,n} + \epsilon^-_{j',n'})(\epsilon^+_{j,n} + \epsilon^-_{j',n'})}\left(\beta - \frac{2}{(\epsilon^+_{j,n} + \epsilon^-_{j',n'})}\right)\Bigg]
$$

$$
+ \Bigg[\frac{nn'(n+1)(n'+1)}{(\epsilon^+_{j,n} + \epsilon^-_{j',n'})(\epsilon^-_{j,n} + \epsilon^+_{j',n'})}\left(\beta - \frac{1}{(\epsilon^-_{j,n} + \epsilon^+_{j',n'})} - \frac{1}{(\epsilon^+_{j,n} + \epsilon^-_{j',n'})}\right)
$$

$$
+ \frac{(n+1)(n'-1)(n+2)n'}{(\epsilon^+_{j,n} + \epsilon^-_{j',n'-1} + \epsilon^+_{j,n+1} + \epsilon^-_{j',n'})(\epsilon^+_{j,n} + \epsilon^-_{j',n'-1})(\epsilon^+_{j,n} + \epsilon^-_{j',n'})}
$$

$$
+ \frac{n(n'+2)(n-1)(n'+1)}{(\epsilon^-_{j,n} + \epsilon^+_{j',n'+1} + \epsilon^-_{j,n-1} + \epsilon^+_{j',n'})(\epsilon^-_{j,n} + \epsilon^+_{j',n'})(\epsilon^-_{j,n} + \epsilon^+_{j',n'})}\Bigg]
$$

$$
+ \Bigg[\frac{nn'(n+1)(n'+1)}{(\epsilon^-_{j,n} + \epsilon^+_{j',n'})(\epsilon^+_{j,n} + \epsilon^-_{j',n'})}\left(\beta - \frac{1}{(\epsilon^-_{j,n} + \epsilon^+_{j',n'})} - \frac{1}{(\epsilon^+_{j,n} + \epsilon^-_{j',n'})}\right)
$$

$$
+ \frac{(n+1)(n'-1)(n+2)n'}{(\epsilon^+_{j,n} + \epsilon^-_{j',n'-1} + \epsilon^+_{j,n+1} + \epsilon^-_{j',n'})(\epsilon^+_{j,n} + \epsilon^-_{j',n'})(\epsilon^+_{j,n} + \epsilon^-_{j',n'})}
$$

$$
+ \frac{n(n'+1)(n-1)(n'+2)}{(\epsilon^-_{j,n} + \epsilon^+_{j',n'} + \epsilon^-_{j,n-1} + \epsilon^+_{j',n'+1})(\epsilon^+_{j',n'} + \epsilon^-_{j,n})(\epsilon^-_{j,n} + \epsilon^+_{j',n'})}\Bigg]
$$

$$
+ \Bigg[\frac{n(n'+2)(n-1)(n'+1)}{(\epsilon^-_{j,n} + \epsilon^+_{j',n'+1} + \epsilon^-_{j,n-1} + \epsilon^+_{j',n'})(\epsilon^-_{j,n} + \epsilon^+_{j',n'})(\epsilon^-_{j,n} + \epsilon^+_{j',n'})}
$$

$$
+ \frac{(n+1)(n'-1)(n+2)n'}{(\epsilon^+_{j,n} + \epsilon^-_{j',n'-1} + \epsilon^+_{j,n+1} + \epsilon^-_{j',n'})(\epsilon^-_{j',n'} + \epsilon^+_{j,n})(\epsilon^+_{j,n} + \epsilon^-_{j',n'})}
$$

$$
+ \frac{(n+1)n'n(n'+1)}{(\epsilon^+_{j,n} + \epsilon^-_{j',n'})(\epsilon^-_{j,n} + \epsilon^+_{j',n'})}\left(\beta - \frac{1}{(\epsilon^+_{j,n} + \epsilon^-_{j',n'})} - \frac{1}{(\epsilon^-_{j,n} + \epsilon^+_{j',n'})}\right)\Bigg]
$$

$$
+ \Bigg[\frac{n(n'+2)(n-1)(n'+1)}{(\epsilon^-_{j,n} + \epsilon^+_{j',n'+1} + \epsilon^-_{j,n-1} + \epsilon^+_{j',n'})(\epsilon^-_{j,n} + \epsilon^+_{j',n'})(\epsilon^-_{j,n} + \epsilon^+_{j',n'})}
$$

$$
+ \frac{(n+1)(n'-1)(n+2)n'}{(\epsilon^+_{j,n} + \epsilon^-_{j',n'-1} + \epsilon^+_{j,n+1} + \epsilon^-_{j',n'})(\epsilon^+_{j,n} + \epsilon^-_{j',n'})(\epsilon^-_{j',n'} + \epsilon^+_{j_1,n_1})}
$$

$$
+ \frac{(n+1)(n'+1)nn'}{(\epsilon^+_{j',n'} + \epsilon^-_{j,n})(\epsilon^+_{j,n} + \epsilon^-_{j',n'})}\left(\beta - \frac{1}{(\epsilon^+_{j',n'} + \epsilon^-_{j,n})} - \frac{1}{(\epsilon^+_{j,n} + \epsilon^-_{j',n'})}\right)\Bigg]
$$

$$+ \left[\frac{n(n'+1)n(n'+1)}{(\epsilon_{j,n}^- + \epsilon_{j',n'}^+)(\epsilon_{j,n}^- + \epsilon_{j',n'}^+)} \left(\beta - \frac{2}{(\epsilon_{j,n}^- + \epsilon_{j',n'}^+)} \right) + \frac{(n+1)n'(n+1)n'}{(\epsilon_{j,n}^+ + \epsilon_{j',n'}^-)(\epsilon_{j,n}^+ + \epsilon_{j',n'}^-)} \left(\beta - \frac{2}{(\epsilon_{j,n}^+ + \epsilon_{j',n'}^-)} \right) \right] \right\} . \quad \text{(B4)}$$

The symmetry of the various terms in and the term-by-term correspondence between Eqs. (B1)–(B4) above are noteworthy. The above results are sufficient for the purposes of this paper, where we discuss only bipartite lattices (specifically, hypercubic lattices in d dimensions with nearest-neighbor hopping only).

---

[1] J. Hubbard, Proc. R. Soc. London, Ser. A **276**, 238 (1963).

[2] M. P. A. Fisher, P. B. Weichmann, G. Grinstein, and D. S. Fisher, Phys. Rev. B **40**, 546 (1989).

[3] K. Sheshadri, H. R. Krishnamurthy, Rahul Pandit, and T. V. Ramakrishnan, Europhys. Lett. **22**, 257 (1993); Phys. Rev. Lett. **75**, 4075 (1995).

[4] D. Jaksch, C. Bruder, J. I. Cirac, C. W. Gardiner, and P. Zoller, Phys. Rev. Lett. **81**, 3108 (1998).

[5] M. Greiner, O. Mandel, T. Esslinger, T. W. Hänsch, and I. Bloch, Nature (London) **415**, 39 (2002).

[6] F. Gerbier, S. Trotzky, S. Foelling, U. Schnorrberger, J. D. Thompson, A. Widera, I. Bloch, L. Pollet, M. Troyer, B. Capogrosso-Sansone, N. V. Prokof'ev, and B. V. Svistunov, Phys. Rev. Lett. **101**, 155303 (2008).

[7] Q. Zhou, Y. Kato, N. Kawashima, and N. Trivedi, e-print arXiv:0901.0606.

[8] J. K. Freericks and H. Monien, Europhys. Lett. **26**, 545 (1994).

[9] J. K. Freericks and H. Monien, Phys. Rev. B **53**, 2691 (1996).

[10] P. B. Weichman, Mod. Phys. Lett. B **22**, 2623 (2008).

[11] R. T. Scalettar, G. G. Batrouni, and G. T. Zimanyi, Phys. Rev. Lett. **66**, 3144 (1991); P. Niyaz, R. T. Scalettar, C. Y. Fong, and G. G. Batrouni, Phys. Rev. B **44**, 7143 (1991); G. G. Batrouni and R. T. Scalettar, *ibid.* **46**, 9051 (1992).

[12] W. Krauth and N. Trivedi, Europhys. Lett. **14**, 627 (1991); W. Krauth, N. Trivedi, and D. Ceperley, Phys. Rev. Lett. **67**, 2307 (1991).

[13] N. Elstner and H. Monien, Phys. Rev. B **59**, 12184 (1999).

[14] N. Elstner and H. Monien, e-print arXiv:cond-mat/9905367.

[15] B. Damski and J. Zakrzewski, Phys. Rev. A **74**, 043609 (2006).

[16] B. Capogrosso-Sansone, S. G. Söyler, N. Prokof'ev, and B. Svistunov, Phys. Rev. A **77**, 015602 (2008).

[17] B. Capogrosso-Sansone, N. V. Prokof'ev, and B. V. Svistunov, Phys. Rev. B **75**, 134302 (2007).

[18] Y. Kato, Q. Zhou, N. Kawashima, and N. Trivedi, Nat. Phys. **4**, 617 (2008).

[19] R. V. Pai, R. Pandit, H. R. Krishnamurthy, and S. Ramasesha, Phys. Rev. Lett. **76**, 2937 (1996).

[20] T. D. Kühner and H. Monien, Phys. Rev. B **58**, R14741 (1998).

[21] T. D. Kühner, S. R. White, and H. Monien, Phys. Rev. B **61**, 12474 (2000).

[22] K. Sengupta and N. Dupuis, Phys. Rev. A **71**, 033629 (2005).

[23] C. Menotti and N. Trivedi, Phys. Rev. B **77**, 235120 (2008).

[24] M. Ohliger and A. Pelster, e-print arXiv:0810.4399.

[25] A. Hoffman and A. Pelster, e-print arXiv:0809.0771.

[26] S. Fölling, A. Widera, T. Müller, F. Gerbier, and I. Bloch, Phys. Rev. Lett. **97**, 060403 (2006).

[27] I. B. Spielman, W. D. Phillips, and J. V. Porto, Phys. Rev. Lett. **98**, 080404 (2007).

[28] I. B. Spielman, W. D. Phillips, and J. V. Porto, Phys. Rev. Lett. **100**, 120402 (2008).

[29] G. D. Mahan, *Many-Particle Physics* (Kluwer Academic/ Plenum, New York, 1981).

[30] P. M. Chaikin and T. C. Lubensky, *Principles of Condensed Matter Physics* (Cambridge University Press, Cambridge, England, 2000).

[31] J. M. Kosterlitz and D. J. Thouless, J. Phys. C **6**, 1181 (1973).

[32] O. F. Syljuasen and A. W. Sandvik, Phys. Rev. E **66**, 046701 (2002).

[33] N. Kawashima and K. Harada, J. Phys. Soc. Jpn. **73**, 1379 (2004).

[34] Y. Kato, T. Suzuki, and N. Kawashima, Phys. Rev. E **75**, 066703 (2007).

[35] Y. Kato and N. Kawashima, Phys. Rev. E **79**, 021104 (2009).

[36] C. Kollath, U. Schollwöck, J. von Delft, and W. Zwerger, Phys. Rev. A **69**, 031601(R) (2004).

[37] N. Teichmann, D. Hinrichs, M. Holthaus, and A. Eckardt, Phys. Rev. B **79**, 100503(R) (2009); e-print arXiv:0904.0905.